Cellular Metabolism Is a Major Determinant of HIV-1 Reservoir Seeding in CD4+ T Cells and Offers an Opportunity to Tackle Infection.

Jose Carlos Valle-Casuso, Mathieu Angin, Stevenn Volant, Caroline Passaes, Valerie Monceaux, Anastassia Mikhailova, Katia Bourdic, Véronique Avettand-Fénoêl, Faroudy Boufassa, Marc Sitbon, et al.

Cellular metabolism is a major determinant of HIV-1 reservoir seeding in CD4+ T cells and offers an opportunity to tackle infection

José Carlos Valle-Casuso[1], Mathieu Angin[1], Stevenn Volant[2], Caroline Passaes[1], Valérie Monceaux[1], Anastassia Mikhailova[1], Katia Bourdic[3], Véronique Avettand-Fenoel[4,5], Faroudy Boufassa[6], Marc Sitbon[7], Olivier Lambotte[3,8], Maria-Isabel Thoulouze[9], Michaela Müller-Trutwin[1], Nicolas Chomont[10] and Asier Sáez-Cirión[1]

[1]Institut Pasteur, Unité HIV Inflammation et Persistance, Paris, France
[2]Institut Pasteur, Hub Bioinformatique et Biostatistique – C3BI, USR 3756 IP CNRS – Paris, France
[3]Assistance Publique Hôpitaux de Paris, Hôpital Bicêtre, Service de Médecine Interne et Immunologie clinique, 94275 Le Kremlin-Bicêtre, France
[4] Université Paris Descartes, Sorbonne Paris Cité, EA7327, Paris, France.
[5] Assistance Publique Hôpitaux de Paris, CHU Necker-Enfants, Laboratoire de Virologie, Malades, Paris, France
[6]INSERM U1018, Centre de recherche en Epidémiologie et Santé des Populations, Université Paris Sud, Le Kremlin Bicêtre, France
[7] Institut de Génétique Moléculaire de Montpellier, University of Montpellier, CNRS, Montpellier, France
[8]CEA, Université Paris Sud, INSERM U1184, Immunology of Viral Infections and Autoimmune Diseases (IMVA), IDMIT Department / IBFJ, Fontenay-aux-Roses, France
[9]Institut Pasteur, Unité Virologie Structurale, Paris, France
[10]Centre de Recherche du CHUM and Department of microbiology, infectiology and immunology, Université de Montréal, H2X0A9, Canada

Lead contact:

Asier Sáez-Cirión: Unité HIV Inflammation et Persistance, Institut Pasteur, 28 rue du Docteur Roux, 75724 Paris Cedex 15, France. Tel.: 33-145-688-768. Fax: 33-145-688-957.
E-mail: asier.saez-cirion@pasteur.fr

ABSTRACT

HIV persists in long-lived infected cells that are not affected by antiretroviral treatment. These HIV reservoirs are mainly located in CD4+ T-cells, but their distribution is variable in the different subsets. Susceptibility to HIV-1 increases with CD4+ T-cell differentiation. We evaluated whether the metabolic programming that supports the differentiation and function of CD4+ T-cells affected their susceptibility to HIV-1. We found that differences in HIV-1 susceptibility between naïve and more differentiated subsets were associated with the metabolic activity of the cells. Indeed, HIV-1 selectively infected CD4+ T-cells with high oxidative phosphorylation and glycolysis, independent of their activation phenotype. Moreover, partial inhibition of glycolysis (i) impaired HIV-1 infection in vitro in all CD4+ T-cell subsets, (ii) decreased the viability of pre-infected cells, and (iii) precluded HIV-1 reactivation in cells from HIV-infected individuals. Our results elucidate the link between cell metabolism and HIV-1 infection and identify a vulnerability to tackle HIV reservoirs.

Keywords: HIV-1, CD4+ T-cell, T cell differentiation, HIV reservoir, susceptibility to HIV-1, glycolysis, oxidative phosphorylation, cellular metabolism, metabolic inhibitors, 2-DG, DON, UK5099

INTRODUCTION

Combination antiretroviral treatment (cART) blocks HIV-1 replication but does not eliminate infected cells. Replication competent HIV-1 persists in cellular reservoirs that are the origin of rapid viral rebound when treatment is interrupted (Finzi et al., 1997). Identifying the factors underlying the seeding and survival of HIV-infected cells is a priority in the search for an HIV cure (Deeks et al., 2016). CD4+ T-cells are the major target for HIV-1 infection and are thought to constitute most of the HIV-1 reservoir. However, not all CD4+ T-cells contribute equally to the pool of persistently infected cells during cART. The composition of CD4+ T-cells that remain infected is mainly determined by the susceptibility of CD4+ T-cell subsets to HIV infection, their resistance to HIV-induced apoptosis and their life span and turnover potential (Barton et al., 2016). Naïve CD4+ T-cells are highly resistant to HIV-1 infection, while HIV-1 susceptibility increases in more differentiated cell subsets (Roederer et al., 1997; Schnittman et al., 1990). Accordingly, there is a minimal contribution of naïve CD4+ T-cells to the HIV reservoir during cART, which is mainly restricted to the memory cell subsets (Chomont et al., 2009). The susceptibility of CD4+ T-cells to HIV-1 infection depends on the relative abundance of cell factors required by the virus to complete its replication cycle and of cellular restriction factors that counteract infection (Lever and Jeang, 2011). T-cell activation sharply increases the expression of HIV dependency factors and thereby cell susceptibility to HIV-1 infection (Pan et al., 2013; Stevenson et al., 1990), despite the concomitant presence of some restriction factors that the virus can most often circumvent. However, responsiveness to TCR activation (Byrne et al., 1988; Roederer et al., 1997) and susceptibility to HIV infection are not homogeneous across or within CD4+ T-cell subsets. This discrepancy in infection efficacy suggests that HIV-1 has adapted to infect CD4+ T-cells with a specific cellular program (Cleret-Buhot et al., 2015). The cellular processes orchestrating the optimal conditions for the establishment of HIV-1 infection remain unclear.

Numerous studies have demonstrated the role of cellular metabolism in T-cell immunity (Pearce et al., 2013; Waickman and Powell, 2012). Naïve T-cells circulate in a quiescent state, relying essentially

on oxidative phosphorylation (OXPHOS). Upon T-cell activation and after receiving appropriate cues (costimulation, cytokines), naïve T-cells undergo metabolic reprogramming, strongly increasing OXPHOS and, especially, glycolysis, to cope with the energy demands of immune function and rapid proliferation (Pearce et al., 2013). The biomass accumulation that accompanies enhanced cellular metabolism may provide viruses with the abundance of factors that are necessary for their replication. It is worth noting that several retroviruses have evolved to use metabolite transporters as cellular receptors. The glucose transporter 1 (GLUT) is the main receptor for HTLV-1 (Manel et al., 2003); phosphate transporters PiT1 and PiT2 have been reported as surface receptors for koala retrovirus, feline leukemia virus and murine leukemia viruses (Oliveira et al., 2006; Takeuchi et al., 1992; von Laer et al., 1998); and the amino acid transporters ASCT1 and ASCT2 are the receptors for the feline RD-114 endogenous retrovirus (Shimode et al., 2013). Although HIV-1 does not use metabolite transporters as its main receptors, GLUT1 expression is necessary for the postentry steps of HIV-1 replication in CD4+ T-cells (Loisel-Meyer et al., 2012). Moreover, the metabolism of nucleotides is critical for HIV-1 reverse transcription (Amie et al., 2013).

In the present study, we undertook the analysis of the conditions determining the intracellular susceptibility of CD4+ T-cell subsets to HIV-1 infection. In particular, we analyzed whether the metabolic program is distinct according to the differentiation of CD4+ T-cell subsets and if this determines their susceptibility to HIV-1 infection. We show that cellular metabolism is a central factor driving the HIV-1 infection of CD4+ T-cells and that it may be an important target for new therapies against HIV-1.

RESULTS

CD4+ T-cell subsets have heterogeneous susceptibility to HIV-1 infection

We first assessed the relative intrinsic susceptibility of primary CD4+ T-cell subsets (naïve, Tn; central memory, Tcm; transitional memory, Ttm; and effector memory, Tem) to HIV-1 infection. We used single-cycle NL4.3ΔenvGFP particles pseudotyped with VSV-G envelope protein (HIV-1_{GFP}-VSV) to circumvent differences in the surface expression of CCR5 across CD4+ T-cell subsets. We activated CD4+ T-cells with soluble anti-CD3. This 'suboptimal' activation protocol has allowed us to expose differences in the susceptibility to HIV-1 of CD4+ T-cells from different individuals that were masked using more potent stimulation protocols (Saez-Cirion et al., 2011). Activation enhanced the susceptibility to HIV-1 without altering the relative contribution of each CD4+ T-cell subset (Figure 1A, B). After infection, the relative frequencies of Tn, Tcm, Ttm and Tem cells among GFP-negative (GFP-) cells was identical to that among noninfected CD4+ T-cells (Figure 1B). In contrast, the composition of HIV-infected GFP-positive (GFP+) cells was different from that of noninfected cells, with a significant exclusion of Tn cells and strong enrichment of Tem cells. Tcm cells were also slightly underrepresented, and Ttm cells were overrepresented among GFP+ CD4+ T-cells when compared to the control condition (Figure 1B). These results suggested different susceptibilities to HIV-1 infection of CD4+ T-cell subsets, with Tem cells being the most susceptible, followed by Ttm and Tcm cells, and with Tn cells being strongly resistant to infection.

To study if these differences were related to the inherent program of each CD4+ T-cell subset, we isolated quiescent CD4+ Tn, Tcm, Ttm and Tem cells (n=6 donors, Figure S1), and we analyzed their susceptibility to HIV-1 with or without activation. Activation enhanced the susceptibility of all CD4+ T-cell subsets to HIV-1 infection (Figure 1C). However, this effect was variable according to the subset. There was a tendency for Tem cells to be more susceptible than other subsets (p=0.06) in the absence of activation, and this difference became more pronounced after three (p=0.0004, all comparisons) or five days of activation (p=0.012, Tem vs Tn and Ttm and Tcm vs Tn and Ttm). Overall,

our results recapitulated previous observations showing an inherent hierarchy in the susceptibility of CD4+ T-cell subsets to HIV-1 infection (Buzon et al., 2014; Tabler et al., 2014).

Levels of HIV infection are related to the molecular program of CD4+ T-cell subsets

To determine if a molecular program was associated with the susceptibility of CD4+ T-cell subsets to HIV infection, we analyzed the expression of a panel of 96 genes (related to T-cell activation, survival, differentiation and function as well as known viral restriction or HIV facilitating factors, Table S1) in each CD4+ T-cell subpopulation at the time of infection. Nonactivated CD4+ T-cell subsets showed distinct transcriptional profiles that were further enhanced after activation (e.g., 34 genes and 49 genes differently expressed between CD4+ T-cell subsets without activation and after 3 days of anti-CD3 treatment, respectively, Figure 2A). These genes were mostly related to signal transduction and the response to stimulus, which could be related to the previously described different susceptibility to CD3 activation of the CD4+ T-cell subsets (Croft et al., 1994; Kumar et al., 2011). The level of HIV-infected cells correlated with the expression of several genes at the time of infection in the different conditions studied (Figure 2B and Figure S2). SAMHD1 showed a negative association with infection. In contrast, positive correlations were observed between infection levels and other antiviral factors (such as APOBEC3G or SLFN11)(Li et al., 2012; Sheehy et al., 2002) as well as several genes involved in the interferon response (IFI6, IFI16, EIF2AK2, and OAS1) (Kane et al., 2016). Significant positive correlations were also observed between the level of HIV infection and the gene expression levels of transcription factors (STAT3, E2F1, and PRDM1), genes that have been proposed to facilitate HIV-1 infection (RRM2, HSP90AA, CFL1, and DYNC1H1)(Allouch et al., 2013; Franke and Luban, 1996; Lukic et al., 2014; Roesch et al., 2012) and multiple genes involved in T-cell metabolism (SLC2A3, SLC2A1, SLC2A5, CASP3, FAS, GAPDH, and GUSB). Taken together, these results suggest that, with the exception of SAMHD1, the antiviral restriction factors analyzed did not decisively influence the cell susceptibility to HIV-1, which is in line with the results of previous reports (Jia et al., 2015). Our data indicate that metabolically active cells may offer favorable conditions for HIV infection.

Hierarchy of susceptibility to HIV infection matches metabolic activity of CD4+ T-cell subsets

To explore the possible association between HIV infection and cell metabolism, we determined the metabolic activity of the CD4+ T-cell subsets at the time of infection. We used a cell flux analyzer to measure, in different conditions, the oxygen consumption rate (OCR) and the extracellular acidification rate (ECAR) as indicators of oxidative phosphorylation (OXPHOS) and glycolysis, respectively (Zhang et al., 2012). In the absence of activation in vitro and in agreement with their quiescent nature, all sorted CD4+ T-cell subsets had low levels of metabolic activity (Figure 3A). Nonetheless, small differences between subsets were noted; basal metabolism and metabolic potential were highest in Tem cells and lowest in Tn cells, while Ttm and Tcm cells presented similar intermediate levels (Figures 3A, B). These differences were more pronounced after activation, with all memory cell subsets increasing mitochondrial function and glycolysis to different extents and with different kinetics. The highest metabolic activity was measured in Tem cells, peaking on day 3 after activation and decreasing on day 5. The metabolism of Ttm and Tcm cells increased after 3 days of activation and then remained stable in Ttm cells while continuing to increase in Tcm cells. In contrast, Tn cells showed a modest increase only in mitochondrial function and not in glycolysis and only after 5 days of activation, when their metabolism was heavily relying on OXPHOS (Figure 3C). Accordingly, important differences were also found between CD4+ T-cell subsets regarding their capacity to uptake glucose and their levels of the surface expression of the GLUT1 receptor, which were lowest in Tn cells and highest in Tem cells (Figures S3A,B). The relative metabolic activity levels of the different cell subsets matched their relative susceptibility to HIV-1 infection (Figure 1C), and we found positive correlations between HIV infection levels and multiple metabolic functions in cells that had been activated (Figure 3D, Figure S3C). These results further point to an influence of the metabolic activity of CD4+ T-cells on their susceptibility to HIV-1.

HIV-infected CD4+ T-cells are characterized by higher levels of metabolic activity independent of cell activation levels

To analyze if there was a direct link between cell metabolism and HIV-1 infection, we challenged 5-day activated bulk CD4+ T-cells with HIV-1_{gfp}-VSV, and we sorted three days later noninfected GFP- and infected GFP+ cells. HIV-infected CD4+ T-cells had higher levels of basal metabolism and metabolic potential and, overall, a more energetic profile than noninfected cells (Figures 4A and S4A). Although we could detect infected cells among cells with low activation levels (Figure 4B), we found higher proportions of GFP+ cells among CD4+ T-cells expressing activation markers. We therefore evaluated whether differences in the metabolic activity of infected and noninfected CD4+ T-cells were just a consequence of the selective infection of CD4+ T-cells with higher activation levels. We sorted CD4+ T-cells first based on their expression of either high or low levels of both HLA-DR and CD25 and then based on whether they were GFP+ or GFP- (Figures 4B and S4). After 5 days of stimulation, the CD4+ T-cell subsets expressed different levels of activation markers (Figure S4B), which were highest in Tem cells and lowest in Tn cells. This was translated to different contributions of CD4+ T-cell subpopulations in the high- and low-activation sorted cell fractions (Figure 4B). Nevertheless, Tn cells were more frequently found in the GFP- fraction, both in high and low-activated cell populations, whereas the GFP+ fraction was enriched with Tem cells. These results matched the hierarchy of infection that we observed before (Figure 1) and further supported that the susceptibility of CD4+ T-cell subsets to HIV-1 depends on the intrinsic characteristics of these cells independent of their activation status. In this regard, we found that infected GFP+ cells in both the high- and low-activation fractions, had higher basal metabolisms (OCR and ECAR) than noninfected GFP- cells (Figure 4C). These results demonstrated that HIV-infected CD4+ T-cells were characterized by higher metabolic activity levels.

HIV-1 infection is preferentially established in CD4+ T-cells with high metabolic activity levels

200 Our results suggest that HIV-1 infection is favored in the environment provided by CD4+ T-cells with
201 high metabolic activity levels. We analyzed if this was due to a selective infection of CD4+ T-cells with
202 the highest metabolic activity levels or if it was HIV-infection that increased the metabolic activity of
203 the cells. We activated CD4+ T-cells and sorted Tn and Tcm cells based on their capacity to uptake
204 high or low levels of the fluorescent glucose analogue 2NBDG (Figure S5A), which corresponded to
205 weakly and strongly glycolytic cells respectively (Figure S5B). We infected these purified cell fractions
206 with HIV-1_{gfp}-VSV. Three days after infection, infected GFP+ CD4+ T-cells were only observed among
207 highly glycolytic Tn and Tcm cells, while weakly glycolytic cells were strongly resistant to infection
208 (65x [41x-206x], median [IQR] fold increase in the proportion of GFP+ cells in HGlu vs LGlu cell
209 subsets, p=0.008) (Figure 5). Overall these results confirmed that, in our conditions, the high
210 metabolic activity of infected CD4+ T-cells was one of the causes rather than a consequence of HIV
211 infection.
212
213 **Suboptimal inhibition of glucose metabolism blocks HIV-1 replication in CD4+ T-cells**
214 The above results indicate that HIV-1 infection of CD4+ T-cells required high levels of metabolic
215 activity. Therefore, we analyzed if HIV-1 replication could be blocked with metabolic inhibitors. We
216 infected activated CD4+ T-cells with HIV-1_{gfp}-VSV in the presence of increasing amounts of etomoxir,
217 an inhibitor of fatty acid oxidation (FAO), 6-diazo-5-oxo-l-norleucine (DON), a glutamine antagonist,
218 or 2-deoxy glucose (2-DG), a competitive inhibitor of glycolysis. Etomoxir was able to reduce HIV
219 infection but only at high concentrations, well above the levels needed to reduce mitochondrial
220 respiration (Figure 6A and Figure S6). DON reduced HIV infection without inducing cell death,
221 although the extent of the inhibition was heterogeneous. Suboptimal amounts of 2-DG (5 mM),
222 which were enough to significantly reduce glycolysis (Figure S6), decreased HIV-1 infection of CD4+ T-
223 cells with minimal cell toxicity (Figure 6A). These results suggested a higher impact of glucose and
224 glutamine metabolism than FAO on HIV-1 replication. The role of glucose metabolism was further
225 confirmed in different sets of experiments in which the frequency of HIV-1-infected CD4+ T-cells was

reduced when the infections were performed in conditions of glucose starvation or in presence of UK5099, a molecule that inhibits the transport of pyruvate, an end product of glycolysis, to the mitochondria (Figure 6B). The presence of 2-DG impaired the accumulation of HIV-1 reverse transcribed products overtime pointing to an early block of viral replication (Figure 6C). 2-DG was able to reduce infection and reverse transcript levels to a similar extent whether it was added to the culture at the time of the challenge or up to 8h later (Figure 6D), indicating that 2-DG was affecting post-entry steps of viral replication. Overall, these results show that a glycolytic environment was necessary for HIV-1 to complete reverse transcription.

2-DG blocked HIV-1 infection in all CD4+ T-cell subsets, although the differences were more pronounced in more differentiated (more glycolytic) cells (Figure 6E). Interestingly, Etomoxir slightly reduced viral replication in Tem cells but not in other T-cell subsets, which could be related to the overall highly energetic nature of these cells. We then used VSV-G pseudotyped NL4.3Δenv Duo-Fluo I particles that allow HIV-1 latently and productively infected cells to be distinguished from each other (Calvanese et al., 2013) (Figure S7A). Interestingly, latent infection was more prominent among Tn and Tcm CD4+ T-cells, while productive infection was predominantly observed among Tem cells (Figure S7A). Overall, the presence of 2-DG significantly reduced the global number of both latently and productively infected CD4+ T-cells (Figure 6F), which agreed with the need for a glycolytic environment for HIV-1 to complete the preintegration steps of its replication cycle.

We then analyzed the impact of inhibition of glycolysis on the infection of CD4+ T-cells with a R5 wild-type replication competent virus (HIV-1 Bal). We first confirmed that the hierarchy of infection of CD4+ T-cell subsets that we observed with VSV-G single cycle particles (Tn<Tcm<Ttm<Tem) coincided with the hierarchy of infection when we used replication competent HIV-1 Bal (Figure S7B). We found that 2-DG was also able to efficiently blocked infection of CD4+ T-cells with HIV-1 Bal (Figure 6G), independently of whether it was added at the time of challenge or 4h/8h after challenge

(Figure S7C). All together, these results show that the inhibition of metabolic activity blocked HIV-1 replication, corroborating that CD4+ T-cell metabolism is an important determinant of HIV-1 infection.

Suboptimal inhibition of glycolysis eliminates HIV-1 infected cells and impairs HIV amplification from CD4+ T-cell reservoirs

We next studied if the preferential establishment of HIV-1 infection in highly glycolytic cells could be used to target HIV-1 reservoirs. First, we analyzed if suboptimal inhibition of glycolysis could selectively eliminate CD4+ T-cells that had been preinfected in vitro. We infected CD4+ T-cells with HIV-1_{gfp}-VSV and sorted infected GFP+ from noninfected GFP- cells (Figure S4A) and cultured them in the absence or presence of 2-DG to inhibit glycolysis. The presence of 2-DG induced higher levels of cell death among infected GFP+ cells than among GFP- cells (Figure 7A and B), affecting all memory T-cell subpopulations (Figure 7C).

As 2-DG was able to both block infection and eliminate infected cells, we wondered whether 2-DG could block HIV spread upon activation of CD4+ T-cells from HIV-infected individuals receiving cART. We isolated CD4+ T-cells from 6 individuals receiving cART (Table S2) and activated the cells with PHA in the absence or presence of 2-DG. In all cases, 2-DG potently blocked HIV-1 amplification, as measured by ultrasensitive analyses of p24 production (Figure 7D). Therefore, the need of HIV for highly glycolytic cells reveals a vulnerability that can be exploited to tackle infection.

DISCUSSION

In this study, we performed a detailed characterization of the bioenergetics of CD4+ Tn, Tcm, Ttm and Tem cells. Upon potent TCR activation, naïve and memory cells have been shown to strongly upregulate their metabolism and acquire effector functions (van der Windt et al., 2013). Here, we show important metabolic differences among the three memory cell populations studied, even in the absence of stimulation. Upon anti-CD3 activation, all CD4+ T-cell subsets enhanced their metabolic activity but essentially maintained their distinctive metabolic programs, which matched the requirements for their expected rapid reaction to antigenic stimulation (Tem>>Ttm>Tcm>>Tn). The metabolic activity of the T-cell subsets overlapped with their susceptibility to HIV-1 infection (Figures 1C and 3B), supporting that the extent of HIV-1 infection in CD4+ T-cell subsets was affected by the metabolic environment within the target cells.

Transcript profiling at the time of infection showed that among the CD4+ T-cell subsets, there were positive correlations between the frequencies of HIV-infected cells and the expression levels of multiple genes related to cell metabolism. Negative correlations were found between the susceptibility of CD4+ T-cells to HIV-1 infection and the expression of SAMHD1, an efficient HIV-1 restriction factor that also plays an important role in the regulation of cell metabolism (Descours et al., 2012; Mathews, 2015). Surprisingly, strong positive correlations were found between the levels of HIV-infected cells and the expression of a cluster of genes related to the interferon response. Although this point was not specifically explored in the present study, increasing evidence has revealed the interrelationships between cell metabolism and the interferon response (Burke et al., 2014; Zhao et al., 2015). Some type 1 interferons might enhance glycolysis (Fritsch and Weichhart, 2016), and interferon regulatory factors play a key role during the metabolic reprogramming that follows TCR-mediated activation of T-cells (Man et al., 2013). The interaction between the interferon response and cell metabolism may somewhat explain the dichotomy between antiviral and viral-enhancing interferon-stimulated genes (Schoggins and Rice, 2011; Seo et al., 2011). Tem cells, which

were the most susceptible to HIV infection in our assay, expressed the strongest levels of several restriction factors such as SLFN11 or APOBEC3G. Our results thus indicate that HIV-1 exploits the metabolic environment that most favors the completion of its replication cycle, and this might be one of the factors underlying the adaptation of HIV-1 to evade some restriction factors.

We further confirmed the association between T-cell metabolism and HIV infection in a series of functional analyses. First, we showed that HIV-infected CD4+ T-cells had higher levels of metabolic activity and metabolic potential than HIV-exposed but noninfected cells. This was not solely the consequence of the preferential infection of cells with higher activation levels; when we sorted CD4+ T-cells that were matched for the expression of common activation markers, we still found that HIV-infected cells had higher metabolic activity levels than noninfected CD4+ T-cells. Although there are well-established links between T-cell activation and cellular metabolism, it is increasingly clear that T-cell functions, including proliferation, the secretion of cytokines and cell survival, are supported through different engagements of the various metabolic pathways (Jones and Bianchi, 2015). This may explain the partial dichotomy between T-cell activation and cell metabolism in HIV infection that we observed in our experiments. Additionally, we found Tn cells expressing high levels of activation markers upon anti-CD3 stimulation, but these cells remained mostly resistant to HIV-1 infection. In contrast, the frequency of infected Tn cells sharply increased when we challenged highly glycolytic Tn cells. This is in agreement with previous results that showed that expression of GLUT1 is necessary for HIV-1 infection of CD4+ T-cells (Loisel-Meyer et al., 2012) and that, in vitro, HIV preferentially infects CD4+ T-cells expressing GLUT1 and OX40 (Palmer et al.). Overall, our results demonstrate that cells that had higher metabolic activity levels were more susceptible to HIV infection.

In our experimental conditions, we could detect virtually no infected cells when we challenged cells with low metabolic activity levels. Thus, any potential change in cell metabolism that might have been induced directly by HIV particles was not sufficient to promote infection in cells that had low

metabolic activity levels at the time of viral challenge. However, it is important to note that because we were interested in understanding the factors modulating HIV infection beyond the expression of HIV receptors, we used single-cycle particles devoid of HIV envelope and pseudotyped with VSV-G in this set of experiments. It is possible that fully replication-competent viruses have a stronger effect on modulating CD4+ T-cell metabolism. CCL5 engagement with CCR5 has been described as increasing glycolysis in T-cells (Chan et al., 2012), and it is possible that gp120 triggers a similar effect. Moreover, HIV infection has been shown to induce increased expression of several glucose transporters in in vitro experiments (Kavanagh Williamson et al., 2018; Sorbara et al., 1996). Overall, viruses appear to possess different mechanisms to enhance cell metabolism to favor viral replication (Goodwin et al., 2015; Sanchez and Lagunoff, 2015), and this deserves additional exploration in the context of HIV infection.

Suboptimal inhibition of glycolysis impaired HIV replication, and this was observed with single-cycle VSVG pseudotyped particles and replication-competent HIV-1 Bal and for all CD4+ T-cell subsets, although the effects were more pronounced in more energetic cells. Inhibition of glycolysis, including several hours after viral entry, severely reduced the accumulation of HIV reverse transcripts and impaired the establishment of both productive and latent infections. Our results thus point to critical steps early during the viral replication cycle (in particular reverse transcription) that are influenced by glycolysis, which agrees with a previous report (Loisel-Meyer et al., 2012). Along these lines, the synthesis of deoxynucleotides, the level of which is a limiting factor for HIV reverse transcription, is very energy demanding and requires substrates that are provided by different metabolic pathways, such as the pentose phosphate pathway (PPP) that is parallel to glycolysis (Lane and Fan, 2015). Although, unfortunately, genes involved in the PPP were not included in our gene expression panel, we found important differences between CD4+ T-cell subsets and strong correlations with infection levels for several genes such as TP53, ESF1 and RRM2, which play critical roles in the de novo synthesis of dNTPs. In particular we have recently shown that changes in the expression of RRM2

impact HIV-1 replication in macrophages and dendritic cells by modifying the pools of dNTPS (Allouch et al., 2013; Valle-Casuso et al., 2017). Moreover, SAMHD1, the expression levels of which were negatively correlated with infection in our analysis, is a deoxynucleoside triphosphohydrolase that contributes to control the intracellular dNTP concentration during cell-cycle (Mathews, 2015). Our results therefore suggest that metabolically active cells offer an environment with positive synthesis (RRM2) vs degradation (SAMHD1) of dNTP pools that favors HIV-1 reverse transcription. However, other steps of the viral replication cycle may also depend on cell metabolism. The inhibition of glycolysis has been shown to decrease the production of HIV-1 particles (Hegedus et al., 2014), and mTOR, a key regulator of cellular metabolism (Waickman and Powell, 2012), appears to be involved in the establishment of HIV-1 latency in CD4+ T-cells (Besnard et al., 2016).

In our functional experiments we mostly focused on assessing the impact of glycolysis on HIV infection. Our results showing that inhibition of pyruvate transport to the mitochondria with UK5099 blocked HIV infection suggests that glucose oxidation is important for HIV-1 infection. However the relative contribution of aerobic vs oxidative glycolysis remains to be determined. It is likely that other metabolic functions are also important for HIV-1 infection. The inhibition of fatty acid oxidation with Etomoxir had a limited effect on HIV replication in suboptimal conditions, mostly in Tem cells, but it strongly inhibited infection at higher concentrations. However, caution is needed when interpreting results obtained with Etomoxir as it has been shown to produce off target effects at such high concentrations (O'Connor et al., 2018; Yao et al., 2018). A recent report suggested that fatty acid metabolism may also participate in the late steps of viral replication (Kulkarni et al., 2017). Our results with the glutamine antagonist DON suggest that glutamine metabolism may also be necessary for the optimal infection of CD4+ T-cells. In general, the association between HIV infection and cell metabolism can be exploited to impair HIV-1 replication.

Cell survival is another process regulated by cell metabolism that could be critically relevant for the persistence of infected cells. We found that suboptimal inhibition of glycolysis induced the selective death of cells that had been preinfected in vitro, and this affected all CD4+ T-cell memory subsets. We also show here that the partial inhibition of glycolysis in CD4+ T-cells from HIV-infected individuals on cART potently blocked viral reactivation and spread. Based on our results, this could be the result of a combination of both the elimination of infected cells and the blocking of new cycles of viral amplification by 2-DG. Overall our results point to the potential modulation of cell metabolism as a strategy to combat HIV infection.

Therapies targeting cellular metabolism are gaining interest in the cancer field (Zhao et al., 2013). Metabolic reprogramming observed in tumor cells closely resembles the metabolic profile of HIV-infected T-cells that we describe here. In the context of the physiopathology of HIV infection, high glucose consumption by infected CD4+ T-cells could have additional implications for immune responses. We recently found that while HIV-specific CD8+ T-cells from rare individuals naturally controlling HIV infection are characterized by metabolic plasticity, HIV-specific CD8+ T-cells from most HIV-infected subjects heavily rely on glycolysis to exert their functions (Angin *et al*, submitted). High levels of glucose consumption by CD4+ T-cells at the sites of viral replication might severely limit glucose availability for these CD8+ T-cells and impair their effector function. In addition, lactic acid, which is a product of glycolysis, inhibits effector functions in cytotoxic T-cells (Mendler et al., 2012). Therefore, the metabolic characteristics of HIV-infected CD4+ T-cells may provide the virus with additional mechanisms to mediate immune evasion, as has also been described for tumors (Sugiura and Rathmell, 2018). Because exploiting the host cell metabolic machinery appears to be a common strategy for invading pathogens, including viruses, bacteria and parasites, therapies targeting cell metabolism could affect a large spectrum of infections. Obviously, cell metabolism regulates critical physiological events, including immune responses, and it is necessary to develop a better understanding of the links between cell metabolism and acute and chronic infections. Overall, our

402 study shows that cellular metabolism is a central factor that drives the HIV-1 infection of CD4+ T-cells
403 more strongly than does the state of differentiation and/or activation, and cellular metabolism may
404 be an important target for new therapies against HIV-1.
405
406 **Limitations of Study**
407 We show here that HIV-1 requires a metabolically rich cellular environment to establish both
408 productive and latent HIV-1 infection in CD4+ T cell subsets. However, our analyses were limited to
409 circulating cells. It remains to be elucidated how this association is affected by the metabolic
410 resources and the particular T-cell programs of the different tissues were HIV-1 replicates. It also
411 remains to be determined if HIV-infected cells sustain the enhanced metabolic activity levels over
412 time, even in the absence of active viral replication, and if this could serve to identify and target
413 persistently infected cells on cART. CD4+ T-cells expressing PD-1 and other immune checkpoints are
414 enriched in HIV in HIV-infected individuals receiving cART (Banga et al., 2016; Chomont et al., 2009;
415 Fromentin et al., 2016). Interestingly, these immune checkpoints appear to mediate their inhibitory
416 activities through the metabolic reprogramming of the cells (Lim et al., 2017; Patsoukis et al., 2015).
417 This suggests that the metabolic requirements of HIV-1 replication might enduringly imprint the
418 infected cells.
419

ACKNOWLEDGEMENTS

The authors wish to thank the study participants for their generous contribution to research. The authors thank the Center for Translational Science (CRT) / Cytometry and Biomarkers Unit of Technology and Service (CB UTechS) at Institut Pasteur for technical support.

FINANCIAL SUPPORT

This study was conducted with funds from the amfAR (108687-54-RGRL and 108928-56-RGRL). JCV-C received support from Sidaction and the Institut Pasteur through the Roux-Cantarini program. MA received support from the EU (under the Marie Sklodowska-Curie grant agreement No 706871) and complementary support from Sidaction. CP received support from the ANRS. AM was supported by the Pasteur-Paris University (PPU) International PhD Program. The ANRS Transbio study is sponsored and funded by the ANRS.

COMPETING FINANCIAL INTERESTS

MS is inventor on patents describing the use of RBD ligands and is the co-founder of METAFORA-biosystems, a start-up company that focuses on metabolite transporters under physiological and pathological conditions. AS-C has received consultancy fees from ViiV healthcare, and speaker fees from MSD, Gilead, BMS and Janssen. MM-T has received speaker fees from Gilead. All the other authors declare no competing financial interests.

AUTHOR CONTRIBUTIONS

JCV-C, VM, MA, CP, AM, VA-F performed experiments; JCV-C, SV and AS-C analyzed the data; KB, FB, MS, M-IT and OL provided key reagents or contributed to the inclusion of study participants and the obtaining and validation of clinical information; JCV-C, NT, MS, MM-T, OL, NC and AS-C contributed to the conception and discussion of the study; JCV-C and AS-C designed the study; AS-C supervised the study; JCV-C and AS-C drafted the article; and all authors critically reviewed the manuscript.

REFERENCES

Allouch, A., David, A., Amie, S.M., Lahouassa, H., Chartier, L., Margottin-Goguet, F., Barre-Sinoussi, F., Kim, B., Saez-Cirion, A., and Pancino, G. (2013). p21-mediated RNR2 repression restricts HIV-1 replication in macrophages by inhibiting dNTP biosynthesis pathway. Proc Natl Acad Sci U S A *110*, E3997-4006.

Amara, A., Vidy, A., Boulla, G., Mollier, K., Garcia-Perez, J., Alcami, J., Blanpain, C., Parmentier, M., Virelizier, J.L., Charneau, P.*, et al.* (2003). G protein-dependent CCR5 signaling is not required for efficient infection of primary T lymphocytes and macrophages by R5 human immunodeficiency virus type 1 isolates. J Virol *77*, 2550-2558.

Amie, S.M., Noble, E., and Kim, B. (2013). Intracellular nucleotide levels and the control of retroviral infections. Virology *436*, 247-254.

Andersen, C.L., Jensen, J.L., and Orntoft, T.F. (2004). Normalization of real-time quantitative reverse transcription-PCR data: a model-based variance estimation approach to identify genes suited for normalization, applied to bladder and colon cancer data sets. Cancer Res *64*, 5245-5250.

Banga, R., Procopio, F.A., Noto, A., Pollakis, G., Cavassini, M., Ohmiti, K., Corpataux, J.M., de Leval, L., Pantaleo, G., and Perreau, M. (2016). PD-1(+) and follicular helper T cells are responsible for persistent HIV-1 transcription in treated aviremic individuals. Nature medicine *22*, 754-761.

Barton, K., Winckelmann, A., and Palmer, S. (2016). HIV-1 Reservoirs During Suppressive Therapy. Trends in microbiology *24*, 345-355.

Besnard, E., Hakre, S., Kampmann, M., Lim, H.W., Hosmane, N.N., Martin, A., Bassik, M.C., Verschueren, E., Battivelli, E., Chan, J.*, et al.* (2016). The mTOR Complex Controls HIV Latency. Cell Host & Microbe *20*, 785-797.

Burke, J.D., Platanias, L.C., and Fish, E.N. (2014). Beta Interferon Regulation of Glucose Metabolism Is PI3K/Akt Dependent and Important for Antiviral Activity against Coxsackievirus B3. J Virol *88*, 3485-3495.

Buzon, M.J., Sun, H., Li, C., Shaw, A., Seiss, K., Ouyang, Z., Martin-Gayo, E., Leng, J., Henrich, T.J., Li, J.Z.*, et al.* (2014). HIV-1 persistence in CD4+ T cells with stem cell-like properties. Nature medicine *20*, 139-142.

Byrne, J.A., Butler, J.L., and Cooper, M.D. (1988). Differential activation requirements for virgin and memory T cells. J Immunol *141*, 3249-3257.

Calvanese, V., Chavez, L., Laurent, T., Ding, S., and Verdin, E. (2013). Dual-color HIV reporters trace a population of latently infected cells and enable their purification. Virology *446*, 283-292.

Chan, O., Burke, J.D., Gao, D.F., and Fish, E.N. (2012). The Chemokine CCL5 Regulates Glucose Uptake and AMP Kinase Signaling in Activated T Cells to Facilitate Chemotaxis. J Biol Chem *287*, 29406-29416.

Chomont, N., El-Far, M., Ancuta, P., Trautmann, L., Procopio, F.A., Yassine-Diab, B., Boucher, G., Boulassel, M.R., Ghattas, G., Brenchley, J.M.*, et al.* (2009). HIV reservoir size and persistence are driven by T cell survival and homeostatic proliferation. Nature medicine *15*, 893-900.

Cleret-Buhot, A., Zhang, Y., Planas, D., Goulet, J.-P., Monteiro, P., Gosselin, A., Wacleche, V.S., Tremblay, C.L., Jenabian, M.-A., Routy, J.-P.*, et al.* (2015). Identification of novel HIV-1 dependency factors in primary CCR4+CCR6+Th17 cells via a genome-wide transcriptional approach. Retrovirology *12*, 102.

494 Croft, M., Bradley, L.M., and Swain, S.L. (1994). Naive versus memory CD4 T cell response
495 to antigen. Memory cells are less dependent on accessory cell costimulation and can
496 respond to many antigen-presenting cell types including resting B cells. J Immunol *152*,
497 2675-2685.
498 David, A., Saez-Cirion, A., Versmisse, P., Malbec, O., Iannascoli, B., Herschke, F., Lucas, M.,
499 Barre-Sinoussi, F., Mouscadet, J.F., Daeron, M.*, et al.* (2006). The engagement of
500 activating FcgammaRs inhibits primate lentivirus replication in human macrophages. J
501 Immunol *177*, 6291-6300.
502 Deeks, S.G., Lewin, S.R., Ross, A.L., Ananworanich, J., Benkirane, M., Cannon, P., Chomont,
503 N., Douek, D., Lifson, J.D., Lo, Y.R.*, et al.* (2016). International AIDS Society global
504 scientific strategy: towards an HIV cure 2016. Nature medicine *22*, 839-850.
505 Descours, B., Cribier, A., Chable-Bessia, C., Ayinde, D., Rice, G., Crow, Y., Yatim, A.,
506 Schwartz, O., Laguette, N., and Benkirane, M. (2012). SAMHD1 restricts HIV-1 reverse
507 transcription in quiescent CD4(+) T-cells. Retrovirology *9*, 87.
508 Finzi, D., Hermankova, M., Pierson, T., Carruth, L.M., Buck, C., Chaisson, R.E., Quinn, T.C.,
509 Chadwick, K., Margolick, J., Brookmeyer, R.*, et al.* (1997). Identification of a reservoir for
510 HIV-1 in patients on highly active antiretroviral therapy. Science *278*, 1295-1300.
511 Franke, E.K., and Luban, J. (1996). Inhibition of HIV-1 replication by cyclosporine A or
512 related compounds correlates with the ability to disrupt the Gag-cyclophilin A
513 interaction. Virology *222*, 279-282.
514 Fritsch, S.D., and Weichhart, T. (2016). Effects of Interferons and Viruses on Metabolism.
515 Front Immunol *7*.
516 Fromentin, R., Bakeman, W., Lawani, M.B., Khoury, G., Hartogensis, W., DaFonseca, S.,
517 Killian, M., Epling, L., Hoh, R., Sinclair, E.*, et al.* (2016). CD4+ T Cells Expressing PD-1,
518 TIGIT and LAG-3 Contribute to HIV Persistence during ART. PLoS Pathog *12*, e1005761.
519 Goodwin, C.M., Xu, S., and Munger, J. (2015). Stealing the Keys to the Kitchen: Viral
520 Manipulation of the Host Cell Metabolic Network. Trends in microbiology *23*, 789-798.
521 Hegedus, A., Kavanagh Williamson, M., and Huthoff, H. (2014). HIV-1 pathogenicity and
522 virion production are dependent on the metabolic phenotype of activated CD4+ T cells.
523 Retrovirology *11*, 98.
524 Jia, X., Zhao, Q., and Xiong, Y. (2015). HIV suppression by host restriction factors and
525 viral immune evasion. Current opinion in structural biology *31*, 106-114.
526 Jones, W., and Bianchi, K. (2015). Aerobic Glycolysis: Beyond Proliferation. Front
527 Immunol *6*.
528 Kane, M., Zang, T.M., Rihn, S.J., Zhang, F., Kueck, T., Alim, M., Schoggins, J., Rice, C.M.,
529 Wilson, S.J., and Bieniasz, P.D. (2016). Identification of Interferon-Stimulated Genes with
530 Antiretroviral Activity. Cell Host Microbe *20*, 392-405.
531 Kavanagh Williamson, M., Coombes, N., Juszczak, F., Athanasopoulos, M., Khan, M.B.,
532 Eykyn, T.R., Srenathan, U., Taams, L.S., Dias Zeidler, J., Da Poian, A.T.*, et al.* (2018).
533 Upregulation of Glucose Uptake and Hexokinase Activity of Primary Human CD4+ T Cells
534 in Response to Infection with HIV-1. Viruses *10*.
535 Kulkarni, M.M., Ratcliff, A.N., Bhat, M., Alwarawrah, Y., Hughes, P., Arcos, J., Loiselle, D.,
536 Torrelles, J.B., Funderburg, N.T., Haystead, T.A.*, et al.* (2017). Cellular fatty acid synthase
537 is required for late stages of HIV-1 replication. Retrovirology *14*, 45.
538 Kumar, R., Ferez, M., Swamy, M., Arechaga, I., Rejas, M.T., Valpuesta, J.M., Schamel, W.W.,
539 Alarcon, B., and van Santen, H.M. (2011). Increased sensitivity of antigen-experienced T
540 cells through the enrichment of oligomeric T cell receptor complexes. Immunity *35*, 375-
541 387.

Lane, A.N., and Fan, T.W.M. (2015). Regulation of mammalian nucleotide metabolism and biosynthesis. Nucleic Acids Res *43*, 2466-2485.
Lever, A.M., and Jeang, K.T. (2011). Insights into cellular factors that regulate HIV-1 replication in human cells. Biochemistry *50*, 920-931.
Li, M., Kao, E., Gao, X., Sandig, H., Limmer, K., Pavon-Eternod, M., Jones, T.E., Landry, S., Pan, T., Weitzman, M.D.*, et al.* (2012). Codon-usage-based inhibition of HIV protein synthesis by human schlafen 11. Nature *491*, 125-128.
Lim, S., Phillips, J.B., Silva, L.M.d., Zhou, M., Fodstad, O., Owen, L.B., and Tan, M. (2017). Interplay between Immune Checkpoint Proteins and Cellular Metabolism. Cancer Res *77*, 1245-1249.
Loisel-Meyer, S., Swainson, L., Craveiro, M., Oburoglu, L., Mongellaz, C., Costa, C., Martinez, M., Cosset, F.-L., Battini, J.-L., Herzenberg, L.A.*, et al.* (2012). Glut1-mediated glucose transport regulates HIV infection. PNAS *109*, 2549-2554.
Lukic, Z., Dharan, A., Fricke, T., Diaz-Griffero, F., and Campbell, E.M. (2014). HIV-1 uncoating is facilitated by dynein and kinesin 1. J Virol *88*, 13613-13625.
Man, K., Miasari, M., Shi, W., Xin, A., Henstridge, D.C., Preston, S., Pellegrini, M., Belz, G.T., Smyth, G.K., Febbraio, M.A.*, et al.* (2013). The transcription factor IRF4 is essential for TCR affinity–mediated metabolic programming and clonal expansion of T cells. Nature Immunology *14*, 1155-1165.
Manel, N., Battini, J.L., and Sitbon, M. (2005). Human T cell leukemia virus envelope binding and virus entry are mediated by distinct domains of the glucose transporter GLUT1. The Journal of biological chemistry *280*, 29025-29029.
Manel, N., Kim, F.J., Kinet, S., Taylor, N., Sitbon, M., and Battini, J.L. (2003). The ubiquitous glucose transporter GLUT-1 is a receptor for HTLV. Cell *115*, 449-459.
Mathews, C.K. (2015). Deoxyribonucleotide metabolism, mutagenesis and cancer. Nat Rev Cancer *15*, 528-539.
Mendler, A.N., Hu, B., Prinz, P.U., Kreutz, M., Gottfried, E., and Noessner, E. (2012). Tumor lactic acidosis suppresses CTL function by inhibition of p38 and JNK/c-Jun activation. Int J Cancer *131*, 633-640.
O'Connor, R.S., Guo, L., Ghassemi, S., Snyder, N.W., Worth, A.J., Weng, L., Kam, Y., Philipson, B., Trefely, S., Nunez-Cruz, S.*, et al.* (2018). The CPT1a inhibitor, etomoxir induces severe oxidative stress at commonly used concentrations. Sci Rep *8*, 6289.
Oliveira, N.M., Farrell, K.B., and Eiden, M.V. (2006). In Vitro Characterization of a Koala Retrovirus. J Virol *80*, 3104-3107.
Palmer, C.S., Duette, G.A., Wagner, M.C.E., Henstridge, D.C., Saleh, S., Pereira, C., Zhou, J., Simar, D., Lewin, S.R., Ostrowski, M.*, et al.* Metabolically active CD4+ T cells expressing Glut1 and OX40 preferentially harbor HIV during in vitro infection. FEBS Lett, n/a-n/a.
Palmer, C.S., Ostrowski, M., Gouillou, M., Tsai, L., Yu, D., Zhou, J., Henstridge, D.C., Maisa, A., Hearps, A.C., Lewin, S.R.*, et al.* (2014). Increased glucose metabolic activity is associated with Cd4+ T-cell activation and depletion during chronic Hiv infection. Aids *28*, 297-309.
Pan, X., Baldauf, H.M., Keppler, O.T., and Fackler, O.T. (2013). Restrictions to HIV-1 replication in resting CD4+ T lymphocytes. Cell Res *23*, 876-885.
Passaes, C.P., Bruel, T., Decalf, J., David, A., Angin, M., Monceaux, V., Muller-Trutwin, M., Noel, N., Bourdic, K., Lambotte, O.*, et al.* (2017). Ultrasensitive HIV-1 p24 Assay Detects Single Infected Cells and Differences in Reservoir Induction by Latency Reversal Agents. J Virol *91*.
Patsoukis, N., Bardhan, K., Chatterjee, P., Sari, D., Liu, B., Bell, L.N., Karoly, E.D., Freeman, G.J., Petkova, V., Seth, P.*, et al.* (2015). PD-1 alters T-cell metabolic reprogramming by

591 inhibiting glycolysis and promoting lipolysis and fatty acid oxidation. Nature
592 Communications *6*, 6692.
593 Pearce, E.L., Poffenberger, M.C., Chang, C.H., and Jones, R.G. (2013). Fueling immunity:
594 insights into metabolism and lymphocyte function. Science *342*, 1242454.
595 Roederer, M., Raju, P.A., Mitra, D.K., Herzenberg, L.A., and Herzenberg, L.A. (1997). HIV
596 does not replicate in naive CD4 T cells stimulated with CD3/CD28. J Clin Invest *99*, 1555-
597 1564.
598 Roesch, F., Meziane, O., Kula, A., Nisole, S., Porrot, F., Anderson, I., Mammano, F., Fassati,
599 A., Marcello, A., Benkirane, M.*, et al.* (2012). Hyperthermia stimulates HIV-1 replication.
600 PLoS Pathog *8*, e1002792.
601 Saez-Cirion, A., Hamimi, C., Bergamaschi, A., David, A., Versmisse, P., Melard, A., Boufassa,
602 F., Barre-Sinoussi, F., Lambotte, O., Rouzioux, C.*, et al.* (2011). Restriction of HIV-1
603 replication in macrophages and CD4+ T cells from HIV controllers. Blood *118*, 955-964.
604 Saez-Cirion, A., Shin, S.Y., Versmisse, P., Barre-Sinoussi, F., and Pancino, G. (2010). Ex
605 vivo T cell-based HIV suppression assay to evaluate HIV-specific CD8+ T-cell responses.
606 Nat Protoc *5*, 1033-1041.
607 Sanchez, E.L., and Lagunoff, M. (2015). Viral activation of cellular metabolism. Virology
608 *479-480*, 609-618.
609 Schnittman, S.M., Lane, H.C., Greenhouse, J., Justement, J.S., Baseler, M., and Fauci, A.S.
610 (1990). Preferential infection of CD4+ memory T cells by human immunodeficiency
611 virus type 1: evidence for a role in the selective T-cell functional defects observed in
612 infected individuals. Proc Natl Acad Sci U S A *87*, 6058-6062.
613 Schoggins, J.W., and Rice, C.M. (2011). Interferon-stimulated genes and their antiviral
614 effector functions. Current Opinion in Virology *1*, 519-525.
615 Seo, J.-Y., Yaneva, R., Hinson, E.R., and Cresswell, P. (2011). Human Cytomegalovirus
616 Directly Induces the Antiviral Protein Viperin to Enhance Infectivity. Science *332*, 1093-
617 1097.
618 Sheehy, A.M., Gaddis, N.C., Choi, J.D., and Malim, M.H. (2002). Isolation of a human gene
619 that inhibits HIV-1 infection and is suppressed by the viral Vif protein. Nature *418*, 646-
620 650.
621 Shimode, S., Nakaoka, R., Shogen, H., and Miyazawa, T. (2013). Characterization of feline
622 ASCT1 and ASCT2 as RD-114 virus receptor. Journal of General Virology *94*, 1608-1612.
623 Sorbara, L.R., Maldarelli, F., Chamoun, G., Schilling, B., Chokekijcahi, S., Staudt, L., Mitsuya,
624 H., Simpson, I.A., and Zeichner, S.L. (1996). Human immunodeficiency virus type 1
625 infection of H9 cells induces increased glucose transporter expression. J Virol *70*, 7275-
626 7279.
627 Stevenson, M., Stanwick, T.L., Dempsey, M.P., and Lamonica, C.A. (1990). HIV-1
628 replication is controlled at the level of T cell activation and proviral integration. EMBO J
629 *9*, 1551-1560.
630 Sugiura, A., and Rathmell, J.C. (2018). Metabolic Barriers to T Cell Function in Tumors. J
631 Immunol *200*, 400-407.
632 Tabler, C.O., Lucera, M.B., Haqqani, A.A., McDonald, D.J., Migueles, S.A., Connors, M., and
633 Tilton, J.C. (2014). CD4+ memory stem cells are infected by HIV-1 in a manner regulated
634 in part by SAMHD1 expression. J Virol *88*, 4976-4986.
635 Takeuchi, Y., Vile, R.G., Simpson, G., O'Hara, B., Collins, M.K., and Weiss, R.A. (1992).
636 Feline leukemia virus subgroup B uses the same cell surface receptor as gibbon ape
637 leukemia virus. J Virol *66*, 1219-1222.
638 Valle-Casuso, J.C., Allouch, A., David, A., Lenzi, G.M., Studdard, L., Barre-Sinoussi, F.,
639 Muller-Trutwin, M., Kim, B., Pancino, G., and Saez-Cirion, A. (2017). p21 Restricts HIV-1

in Monocyte-Derived Dendritic Cells through the Reduction of Deoxynucleoside Triphosphate Biosynthesis and Regulation of SAMHD1 Antiviral Activity. J Virol *91*.
van der Windt, G.J., O'Sullivan, D., Everts, B., Huang, S.C., Buck, M.D., Curtis, J.D., Chang, C.H., Smith, A.M., Ai, T., Faubert, B.*, et al.* (2013). CD8 memory T cells have a bioenergetic advantage that underlies their rapid recall ability. Proc Natl Acad Sci U S A *110*, 14336-14341.
von Laer, D., Thomsen, S., Vogt, B., Donath, M., Kruppa, J., Rein, A., Ostertag, W., and Stocking, C. (1998). Entry of Amphotropic and 10A1 Pseudotyped Murine Retroviruses Is Restricted in Hematopoietic Stem Cell Lines. J Virol *72*, 1424-1430.
Waickman, A.T., and Powell, J.D. (2012). mTOR, metabolism, and the regulation of T-cell differentiation and function. Immunol Rev *249*, 43-58.
Yao, C.H., Liu, G.Y., Wang, R., Moon, S.H., Gross, R.W., and Patti, G.J. (2018). Identifying off-target effects of etomoxir reveals that carnitine palmitoyltransferase I is essential for cancer cell proliferation independent of beta-oxidation. PLoS Biol *16*, e2003782.
Zhang, J., Nuebel, E., Wisidagama, D.R., Setoguchi, K., Hong, J.S., Van Horn, C.M., Imam, S.S., Vergnes, L., Malone, C.S., Koehler, C.M.*, et al.* (2012). Measuring energy metabolism in cultured cells, including human pluripotent stem cells and differentiated cells. Nat Protoc *7*, 1068-1085.
Zhao, G.-N., Jiang, D.-S., and Li, H. (2015). Interferon regulatory factors: at the crossroads of immunity, metabolism, and disease. Biochimica et Biophysica Acta (BBA) - Molecular Basis of Disease *1852*, 365-378.
Zhao, Y., Butler, E.B., and Tan, M. (2013). Targeting cellular metabolism to improve cancer therapeutics. Cell Death & Disease *4*, e532.

FIGURE LEGENDS

Figure 1. CD4+ T-cells subsets have different susceptibilities to HIV-1 infection

A) Representative example of the proportion of 5-days activated CD4+ T cells expressing GFP in the absence of infection (top) or 72 h after challenge with HIV-1_{GFP}-VSV (bottom). B) Relative distribution of CD4+ T-cell subsets in nonactivated (NA) and activated (aCD3 5d) cells before HIV challenge and in activated cells not expressing GFP (aCD3 5d GFP-) or expressing GFP (aCD3 5d GFP+) 72 h post challenge. The pie charts (top) represent the median values (n=3 donors). The bottom panels represent the fold change in the CD4+ T-cells subset contribution relative to the nonactivated condition (NA). *$p<0.05$; ** $p<0.01$. In a different set of experiments, sorted CD4+ T-cell subsets were cultured under NA or activated conditions for 3 (3d) or 5 days (5d) and challenged with HIV-1_{GFP}-VSV. C) Representative example of infection levels in Tn, Tcm, Ttm and Tem cells from a donor in the different conditions analyzed. D) Medians and IQR values for experiments with cells from 6 donors. Symbols represent the individual data points. Significant differences between experimental conditions are shown for each T-cell subset as horizontal lines. The median infection level in NA Tn cells is displayed as a reference dashed line to facilitate comparison between T-cell subsets.

Figure 2. HIV-1 infection levels in CD4+ T-cell subsets correlate with the expression levels of genes related to cell metabolism

A) Heat maps displaying the genes differentially expressed ($p<0.05$) between the CD4+ T-cell subsets (Tn, Tcm, Ttm and Tem) (n= 6 donors) in the absence of activation or after 3 or 5 days of activation with soluble anti-CD3 (i.e., at the time of HIV challenge) (green = downregulation, red = upregulation). Variables are ordered by hierarchical clustering and samples by CD4+ T-cell subsets. B) Spearman's correlation between the levels of gene expression at the time of HIV-1 challenge and HIV-1 infection levels 72 h after challenge. Only significant correlations ($p<0.05$) are represented in the graphs (green bars). Genes highlighted in red show the group of genes that correlated with infection levels in all conditions.

Figure 3. CD4+ T-cell subsets have different metabolic profiles that coincide with their susceptibility to HIV-1 infection

OCR and ECAR in nonactivated (NA), 3-day activation (3d) and 5-day activation (5d) CD4+ T-cell subsets. A) Median values of the metabolic variables obtained for the CD4+ T-cell subsets from the 6 donors in the different conditions analyzed. B) Median and IQR basal OCR (left panel) and ECAR (right panel) and C) basal ECAR/OCR ratio for CD4+ T-cell subsets in different activation states (0d, 3d, 5d). Median values in NA Tn cells are indicated by dashed lines as a reference. Symbols represent independent experiments (n=6). D) Summary of correlations between metabolic parameters at the time of infection in NA, 3d and 5d activated CD4+ T-cell subsets and the % of infected cells 72 h post infection. The green color indicates $p<0.05$. The size of the circle represents Spearman's coefficients.

Figure 4. HIV-1-infected CD4+ T-cells are characterized by higher metabolic activity levels

A) Metabolic activity (OCR and ECAR) of sorted HIV-infected GFP+ and noninfected GFP- CD4+ T-cells (n=3). A. The bioenergetic (XF) phenotypes of GFP+ and GFP- cells (right panel) were determined by the basal OCR and ECAR values. The symbols represent independent experiments (n=3 donors). B) In a different set of experiments, CD4+ T-cells were sorted 72 h after HIV challenge based first on their activation levels (high activation, CD25+/HLA-DR+ or low activation, CD25-/HLA-DR-) and then on the level of GFP expression (GFP- or GFP+ cells). The gating strategy is shown on the left panels. Pie charts (right) represent the median (n=4 donors) distribution of the CD4+ T-cell subsets (determined by flow cytometry) for each sorted cell fraction as follows: high activation and GFP+, high activation and GFP-, low activation and GFP+ and low activation and GFP- (n=4). C) Representative analyses of OCR and ECAR (measured as above) for each cell fraction (left) and the median and IQR basal OCR and ECAR for 6 (high activation) and 4 (low activation) donors (right).

Figure 5. Rate of glucose uptake by CD4+ T-cell subsets is associated with their susceptibility to HIV-1 infection

CD4+ T cells were sorted based on their differentiation status (Tn or Tcm) and their rate of 2NBDG uptake. Sorted cells were then challenged with HIV-1_{GFP}-VSV. A) Representative example of 2NBDG content after sorting (top panels) and the levels of GFP expression 72 h after challenge in CD4+ T-cell fractions exposed (HIV-1) or not (control) to the virus. B) Percentage of GFP-positive cells among CD4+ T-cell fractions (Tn and Tcm sorted depending on their preinfection 2-NBDG uptake). Symbols represent individual values (n=3, Tn; n=5, Tcm) donors. Medians and IQR values are represented by horizontal lines.

Figure 6. Inhibition of cell metabolic pathways blocks HIV-1 infection of CD4+ T-cells

A) Relative level of infection (blue bars) and cell death (purple bars) compared to the control conditions in 5-days activated CD4+ T-cells infected in the absence or presence of increasing amounts of Etomoxir, DON, or 2-DG (median and IQR, n=3 donors). B) Infection and cell death in CD4+ T-cells exposed to HIV-1 in glucose-containing medium in the absence or presence of 2-DG (5 mM) or in culture medium without glucose (starvation) (left) or in the absence or presence of UK5099 (25 µM) (right). C) Relative number of U5-Gag copies in CD4+ T-cells at 6h, 15h or 72h after infection with HIV-1_{GFP}-VSV in the absence or presence of 2-DG. Individual values (symbols), medians and IQRs (horizontal lines) for five different donors are shown. D) Infection levels and number of U5-Gag copies 72h after challenge with HIV-1_{GFP}-VSV in the absence or presence of 2-DG added at the time of challenge, 4h or 8h post challenge. Values represent the relative levels of infection compared to the control condition (median and IQR, n=3 donors). E) Changes in HIV-1 infection levels in CD4+ T-cell subsets 72h after the infection of bulk CD4+ T-cells in the absence or in presence of 2-DG (orange symbols) or Etomoxir (beige symbols). Medians (n=7 donors) are shown. F) Percentage of HIV-1 productively (left panel) or latently (right panel) infected cells 72h after the infection of CD4+ T-cells with HIV-1DuoFluo VSVG particles in the presence of 2-DG or etomoxir. Median and IQR values from

experiments with 6 donors are shown. G) p24 production in supernatants from CD4+T-cell cultures 3 and 7 days after infection with HIV-1 BaL in the absence (blue bars) or presence of 2-DG (5 mM) (orange bars). Means and standard deviations for three replicates are shown at each time point for experiments done with cells from three different donors.

Figure 7. Suboptimal inhibition of glucose metabolism selectively eliminates preinfected CD4+ T-cells and inhibits HIV-1 amplification from reservoirs

A) Cell viability in sorted pre-infected GFP+ (green) or noninfected GFP- (red) CD4+ T cells cultured for 48 h in the absence or presence of 2-DG. A) One representative example is shown. B) Relative survival of 2-DG treated cells (circles) was compared to that of nontreated cells (squares) at 24 h and 48 h. C) Changes in the CD4+ T-cell subset distribution 48h after the treatment of infected bulk CD4+ T-cells with 2-DG when compared with the distribution in the control condition. Median values and IQR are shown (n=3 donors). D) HIV-1 reactivation from CD4+ T-cells from six individuals on cART upon PHA/IL-2 stimulation in the absence (blue line/symbols) or presence of 2-DG (5 mM) (orange line/symbols) (mean and SD, 3 replicates). Mean p24 values in the absence or presence of 2-DG on day 14 post stimulation are shown for all six experiments (right panel).

STAR METHODS

CONTACT FOR REAGENT AND RESOURCE SHARING

Further information and requests for resources and reagents should be directed to the Lead Contact, Asier Saez-Cirion (asier.saez-cirion@pasteur.fr). Request for biological resources will be fulfilled based on availability and upon the establishment of an MTA.

EXPERIMENTAL MODEL AND SUBJECT DETAILS

Blood samples from non-HIV-infected donors were obtained from the French blood bank (Etablissement Français du Sang) as part of an agreement with the Institut Pasteur (C CPSL UNT, number 15/EFS/023). Fifty-milliliter blood samples were obtained from six HIV-infected individuals on antiretroviral therapy who had HIV plasma viral loads <50 RNA copies/mL from the ANRS TRANSbioHIV study after obtaining written informed consent in accordance with the Declaration of Helsinki (Table S2). The TRANSbioHIV study was approved by the Ethics Review Committee (Comité de protection des personnes) of Île-de-France VII.

METHOD DETAILS

Isolation and culture of CD4+ T-cells

CD4+ T-cells were purified (>90%) from freshly isolated PBMCs by negative selection with antibody-coated magnetic beads (EasySep™ Human CD4+ T-cell Enrichment Kit Ref.19052) in a Robosep instrument (Stem Cell Technology).

Purified CD4+ cells (10^6 cell/mL) were cultured in RPMI 1640 containing GlutaMAX, 10% FCS, penicillin (10 IU/mL) and streptomycin (10 µg/mL) in the presence of IL-2 (Miltenyi) at 50 IU/mL (Culture media). Depending on the experiment, cells were left unstimulated or were stimulated for 3 or 5 days with 0.5 µg/mL soluble antiCD3 (BioLegend, Ref.300414, Clone UCHT1) in the absence of CD28 co-stimulation as previously described (Saez-Cirion et al., 2011). Different compounds that target metabolic pathways [2-deoxy-glucose, 2-DG (Seahorse Biotechnologies); (+)-Etomoxir sodium

786 salt hydrate (Sigma, Ref. E1905); UK5099 (Sigma, Ref. PZ0160); 6-diazo-5-oxo-l-norleucine
787 (DON)(Sigma, Ref. D2141); glucose (Seahorse Biotechnologies); oligomycin (Seahorse
788 Biotechnologies) or carbonyl cyanide 4-(trifluoromethoxy)phenylhydrazone FCCP (Seahorse
789 Biotechnologies)] were added to the culture media at different times and concentrations depending
790 on the protocol conditions. A glucose-free culture media was used in some infection experiments and
791 is described in the results section [RPMI non-glucose, GlutaMAX, containing 10% FCS, penicillin (10
792 IU/mL) and streptomycin (10 µg/mL) in the presence of IL-2 (Miltenyi) at 50 IU/mL (culture media)].
793 After culture, living cells were counted with an automatic Countess cell counter (Invitrogen) based on
794 size and non-staining with trypan blue. The number of living cells was then normalized before
795 analysis.
796
797 **HIV infection in vitro**
798 Single-round infections were performed with HIV-1 NL4.3ΔenvΔnef/GFP (Amara et al., 2003) and
799 HIV-1-DuoFluoΔenv(R7GEmC) (provided by Professor Eric Verdin and Dr. Calvanese, NIH AIDS
800 Reagent Program, Division of AIDS, NIAID, NIH: Cat# 12595 DuoFluo (R7GEmC)) (Calvanese et al.,
801 2013). Both viruses were pseudotyped with the VSV-G envelope protein by transiently cotransfecting
802 (SuperFect; Qiagen) 293T cells with the proviral vectors and the VSV-G expression vector pMD2.G.
803 Nonactivated or activated CD4 + T-cells were infected in triplicate ($5x10^4$ cells/well, 200 µL) with 35
804 ng/$1x10^6$ HIV-1 NL4.3Δnef/GFP/VSV-G and with 70 ng of HIV-1-DuoFluo(R7GEmC)/VSVg per million
805 cells. Active HIV-1 infection was estimated by flow cytometry (BD LSRII, BD bioscience) as the
806 percentage of GFP-expressing CD4+ T-cells 72 h after infection. Latent HIV infection was estimated by
807 flow cytometry as the percentage of mCherry+GFP-CD4+ T-cells 72 h after infection with HIV-1-
808 DuoFluo(R7GEmC) particles.
809
810 HIV-1 reverse transcripts (U5-Gag) were quantified by real-time PCR with an Applied Biosystems 7500
811 Real-Time PCR System 6, 16 and 72 h after infection of CD4+ T-cells with VSV-G–pseudotyped HIV-1

particles as described in (David et al., 2006). Briefly, total DNA was extracted with the NucleoSpin 8/96 Tissue Core kit (Macherey-Nagel, Ref. 740453.4) and 100 ng of template DNA were used per reaction. DNA loading was controlled by concurrently amplifying the albumin gene by real-time PCR and quantifying with reference to a control human genomic DNA (Roche). The reaction mixture contained 1× TaqMan Universal PCR master mix, 300 nM of primers and 200 nM of the fluorogenic probe, in a final volume of 30 µl. PCR cycle conditions were: 50°C for 2 min, 95°C for 10 min, and 40 cycles of 95°C for 15 s and 60°C for 1 min. Copy numbers of U5-Gag were determined with reference to a standard curve prepared by concurrent amplification of serial dilutions of 8E5 cells containing one integrated copy of HIV-1 per cell.

Productive HIV-1 infection in vitro was studied in suboptimally activated CD4+ T-cells (10^6 cells/mL in triplicate) exposed to the HIV-1 BaL strain (R5) (10 ng p24/ml). The cells were cultured in 96-U-well plates for 14 days in the presence or absence of 2-DG (5 mM). Every 3-4 days, the culture supernatants were removed and replaced with fresh culture medium with or without 2-DG. Viral replication was monitored in the supernatants by p24 enzyme-linked immunosorbent assay (ELISA) (XpressBio) or at day 3 by intracellular p24 staining (p24-FITC (clone KC57, Coulter) (Saez-Cirion et al., 2010).

Flow-assisted sorting of CD4 + T-cell subsets

Cells were first selected based on size and structure to eliminate cellular debris. Then cell singlets and living cells (not stained with LIVE/DEAD Fixable Aqua Dead Cell Stain Kit, Thermofisher) are gated before proceeding with further selection based on phenotypical or functional markers (Figures S1, S4, S5).

Resting (CD25-, CD69-, HLA-DR-) CD4+ T-cell subsets [naïve (**Tn**; CD3+, CD4+, CD45RA+, CCR7+, CD27+, CD95-), central memory (**Tcm**; CD3+, CD4+, CD45RA-, CCR7+, CD27+), transitional memory

(**Ttm**; CD3+, CD4+, CD45RA-, CCR7-, CD27+) or effector memory (**Tem**; CD3+, CD4+, CD45RA-, CCR7-, CD27-)] were sorted on a FACS ARIA III cell sorter (BD) using the following antibody panel: CD3-eFLuor450 (eBioscience), CD4-alexaFluor700 (BD), CD45RA-ECD (BC), CCR7-PE_Cy7 (BioLegend), CD27-APC (Miltenyi), CD95-PE (Miltenyi), CD25-FITC (BD), CD69-FITC (eBioscience) and HLA-DR-FITC (BD). The gating strategy is depicted in Figure S1. The number of sorted cells varied from 0.5 to 5 million cells depending on the CD4+ T-cell subset and the donor. The purity of the sorted subset was greater than 98%.

GFP+ and GFP- CD4+ T-cells were sorted 72 h after infection with VSV-G pseudotyped NL4.3ΔenvΔnef/GFP particles (Figure S4A). For some experiments, GFP+ and GFP- cells were also sorted into the following categories based on their expression of activation markers (CD25-ECD, HLA-DR_PerCyP5.5) (Figure 4 and Figure S4B): high activation GFP+ [**H/+** (GFP+, CD25+,HLA-DR+)]; high activation GFP- [**H/-** (GFP-, CD25+, HLA-DR+)]; low activation GFP+ [**L/+**, (GFP+, CD25-,HLA-DR-)]; and low activation GFP- [**L/-** (GFP-, CD25-,HLA-DR-)].

For some experiments, CD4+ Tn and Tcm cells were sorted based on their level of glucose uptake after 5 days of stimulation with anti-CD3 (Figure S5A). The cells were washed and incubated with 2-NBDG (2-(N-(7-nitrobenz-2-oxa-1,3-diazol-4-yl)amino)-2-deoxyglucose) (Thermo Fisher, Ref. N13195) at 75 µM in PBS for 30 min at 37°C. After 3 washes of 10 min each with fresh PBS, the cells were stained with antibodies (CD3-eFLuor450 (eBioscience), CD4-alexaFluor700 (BD), CD45RA-ECD (BC), CCR7-PE_Cy7 (BioLegend), and CD27-APC (Miltenyi)) and sorted as follows: **Tn HGlu** (CD3+, CD4+, CD45RA+, CCR7+, CD27+, 2NBDG+); **Tn LGlu** (CD3+, CD4+, CD45RA+, CCR7+, CD27+, 2NBDG-); **Tcm HGlu** (CD3+, CD4+, CD45RA-, CCR7+, CD27+, 2NBDG+); and **Tcm LGlu** (CD3+, CD4+, CD45RA-, CCR7+, CD27+, 2NBDG-).

Surface GLUT1 staining

CD4+ T-cells were stained with HRBD-rFc, a recombinant fusion protein that specifically binds GLUT1 (Metafora-biosystems, Paris, France), and a secondary goat-anti-Mouse Alexa Fluor 647 antibody (Thermofisher). HRBD is derived from the receptor-binding domain of the human T-cell leukemia virus envelope glycoprotein that binds the extracellular domain of GLUT1 (Manel et al., 2005). The following antibody panel was used to determine CD4+T cell subsets: CD3-eFLuor450 (eBioscience), CD4-alexaFluor700 (BD), CD45RA-ECD (BC), CCR7-PE_Cy7 (BioLegend), CD27-PE (BD bioscience).

Quantitative RT-PCR arrays

The expression levels of an array of 96 genes in the CD4+ T-cell subsets were quantified by RT-qPCR with a Biomark HQ system. Total RNA was extracted from $5x10^4$ CD4+ T-cells with an RNA trace kit (Macherey-Nagel, Ref. 740731.4) and treated with DNase, following the manufacturer's instructions. Twenty microliters of RNA (> 10 ng) was reverse transcribed with Reverse Transcription Master Mix (Fluidigm, 100-6298) (5 minutes at 25°C, 30 minutes at 42°C, and 5 minutes at 85°C). A specific target preamplification (STA) was performed by adding PreAmp Master Mix, 96 Primers Mix and EDTA to the cDNA, followed by STA cycling (95°C: 2 min, 18 cycles of [96°C: 5 s, 60°C 4 min]). The sample was then treated with exonuclease I (New England Biolabs) (37°C: 30 min, 80°C: 15 min). Sample premix (SsoFast EvaGreen Supermix with Low ROX (Biorad), DNA Binding Dye (Fluidigm), preamplified Exo 1-treated sample) and assay mix (assay loading reagent (Fluidigm), Delta Gene primers (Fluidigm)) were then loaded on primed 96.96 Dynamic Array chips (Fluidigm). The chips were transferred into a Biomark HQ device (Fluidigm) for thermocycling, and fluorescence was acquired with the GE 96×96 PCR+Melt v2 program. Linear derivative mode baseline correction was applied. We used the Normfinder algorithm (Aarhus University Hospital, Denmark) (Andersen et al., 2004) to identify the optimal normalization gene among the assayed candidates for our experimental conditions. BENC1 was thus identified as the optimal normalization gene based on expression stability in the analyzed samples (Table S3), and the gene expression values were plotted as $2^{-\Delta\Delta Ct}$, where $\Delta\Delta Ct = \Delta Ct_{SAMPLE} - \Delta Ct_{CONTROL}$, and $\Delta Ct = Ct_{TARGET\ GENE} - Ct_{BENC1}$.

890

891 **Measurement of oxygen consumption and extracellular acidification rates**

892 The oxygen consumption rate (OCR) and extracellular acidification rate (ECAR) were measured using
893 a Seahorse XF96 metabolic analyzer following the procedure recommended by the manufacturer.
894 Briefly, for all the experiments, different CD4+ T-cell populations were seeded at a concentration of
895 2×10^5 cells per well on XF96 plates (Seahorse Bioscience) precoated with 0.5 mg/ml Cell Tack
896 (Corning, Ref. 354240) immediately before adding Seahorse XF culture media to each well. Cells were
897 incubated for 50 min in a CO_2-free incubator at 37°C before loading the plate in the Seahorse
898 analyzer. Different programs were run on the Seahorse analyzer depending on the assay. Drug Panel
899 A (1) XFmedia 2) oligomycin (2.5 µM), 3) FCCP (0.9 µM) and 4) rotenone (1 µM) and antimycin A (1
900 µM)) was injected through ports A, B, C and D, respectively, for the mitochondrial stress test. Drug
901 Panel B (1) XFmedia 2) glucose (10 mM) 3) oligomycin (2.65 µM), and 4) 2-DG (100 mM)) was used
902 for the glycolysis stress test.

903

904 **Phenotyping after sorting**

905 In some experiments, sorted GFP+/- CD4+ T-cells subset or CD4+ T bulk cells previously infected with
906 NL4.3Δnef/GFP/VSV-G with or without 2-DG or Etomoxir were incubated with CD3-eFLuor450
907 (eBioscience), CD4-alexaFluor700 (BD Biosciences), CD45RA-ECD (BC), CCR7-PE_Cy7 (BioLegend) and
908 CD27-APC (Miltenyi) to determine the CD4+ T-cell subset distribution. In addition, the activation
909 levels of sorted CD4+ T-cell subsets were assessed with CD25-ECD (BD Biosciences) and HLA-DR-FITC
910 (BD Biosciences). For both protocols, cells were incubated with the antibodies for 25 minutes and
911 then washed in PBS plus 1% FCS and fixed in 4% paraformaldehyde for flow cytometry on an LSRII
912 device (BD Biosciences). The data were analyzed with Kaluza software (Beckman Coulter).

913

914 **HIV-1 reactivation in CD4+ T-cells from HIV-1-infected individuals.**

915 Freshly isolated CD4+T-cells (negative selection kit, Stem Cell) from HIV-individuals undergoing
916 successful cART were seeded in 48-well plates ($1x10^6$ cells/well, in triplicate) and stimulated with
917 phytohemagglutinin-L (PHA-L, Roche, 1 µg/mL) and IL-2 (Miltenyi) 100UI with or without 2-DG (5
918 mM). The culture supernatants were collected every 3 to 4 days, and fresh medium +/- 2-DG was
919 added to the cultures. Supernatants were stored at -80°C, and HIV-1 p24 was analyzed later by
920 ultrasensitive digital ELISA (Simoa, Quanterix) (Passaes et al., 2017).
921
922 **QUANTIFICATION AND STATISTICAL ANALYSIS**
923 **Differential gene expression**
924 For each gene, we implemented a mixed effects model to detect differential expression between cell
925 types (Tn, Tcm, Ttm and Tem). We defined a model that included the type of cells as a fixed effect
926 and the patient as a random effect. A p-value was then obtained by implementing a likelihood ratio
927 test between the full model and a reduced model without the fixed effect. Heat maps were
928 generated by K-means clustering. Data were filtered by variance ($\delta/\delta max=0.2$) to reduce background
929 noise. Gene expression data were centered to a mean value of zero and scaled to unit variance.
930
931 **Correlation between gene expression, metabolic parameters and HIV-1 susceptibility**
932 We computed Spearman's correlation coefficient and tested for significance.
933
934 **Other analyses**
935 Values are presented in the graphs as medians and interquartile ranges. Statistical analyses were
936 performed using SigmaPlot (Systat Software). The asterisks represent statistically significant
937 differences (*$p<0.05$; ** $p<0.01$). Differences between CD4+ T-cell subsets in different conditions
938 were analyzed with nonparametric signed ANOVA and the multiple comparison Student-Newman-
939 Keuls method. Differences between GFP+ and GFP- CD4+ T-cells or control vs treatment culture
940 conditions were analyzed with paired t-tests. When multiple treatment conditions were tested,

941 ANOVA analyses and the Holm-Sidak method for multiple comparisons versus control group were
942 used, and significant differences between experimental conditions were shown as horizontal lines.
943
944

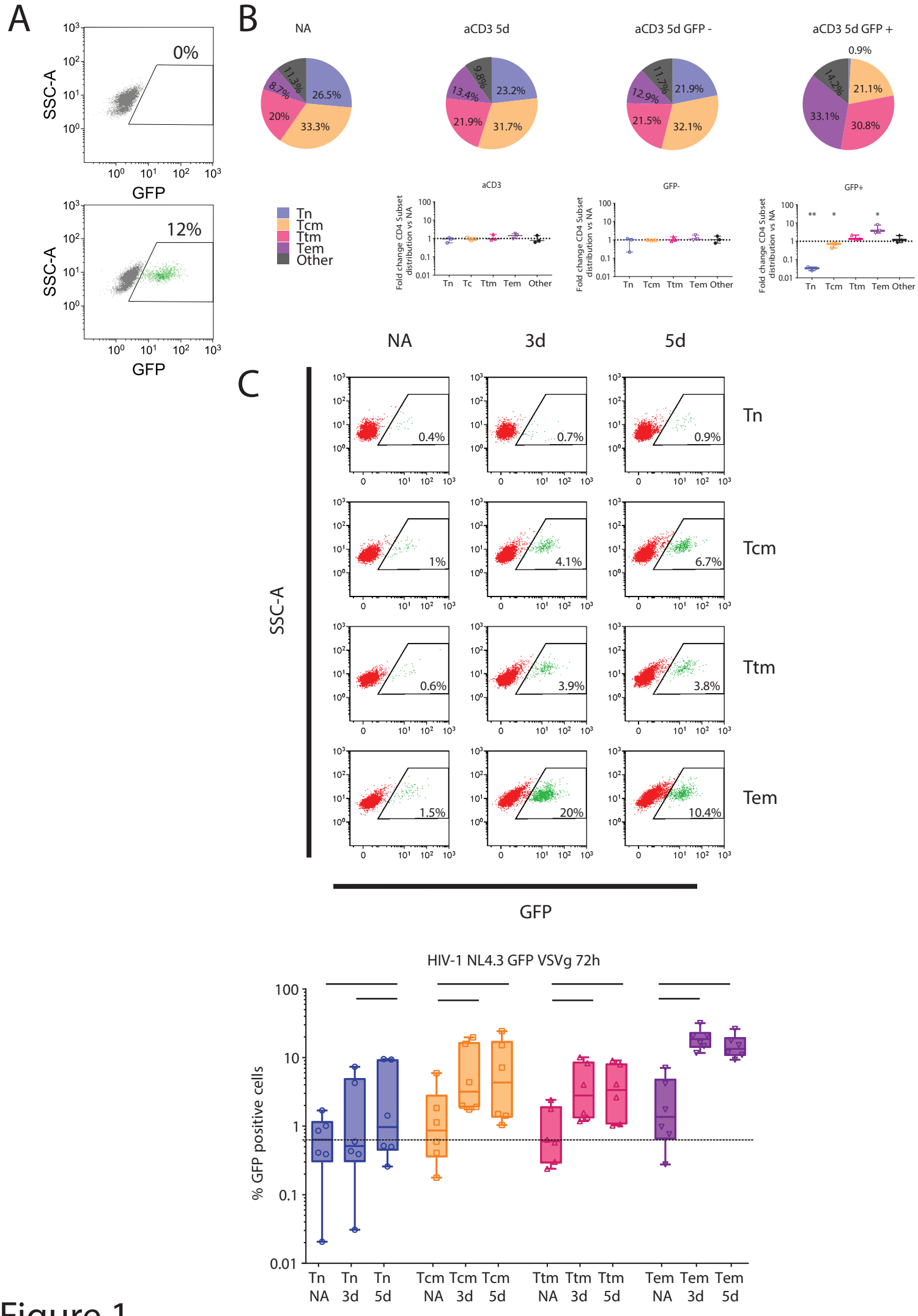
A
SSC-A
GFP
0%
12%
B
NA
aCD3 5d
aCD3 5d GFP -
aCD3 5d GFP +
26.5%
33.3%
20%
8.7%
11.3%
23.2%
31.7%
21.9%
13.4%
9.8%
21.9%
32.1%
21.5%
12.9%
11.7%
0.9%
21.1%
30.8%
33.1%
14.2%
Tn
Tcm
Ttm
Tem
Other
aCD3
GFP-
GFP+
Fold change CD4 Subset distribution vs NA
Tn Tc Ttm Tem Other
Tn Tcm Ttm Tem Other
C
NA
3d
5d
SSC-A
GFP
0.4%
0.7%
0.9%
1%
4.1%
6.7%
0.6%
3.9%
3.8%
1.5%
20%
10.4%
HIV-1 NL4.3 GFP VSVg 72h
% GFP positive cells
Tn NA
Tn 3d
Tn 5d
Tcm NA
Tcm 3d
Tcm 5d
Ttm NA
Ttm 3d
Ttm 5d
Tem NA
Tem 3d
Tem 5d

Figure 1

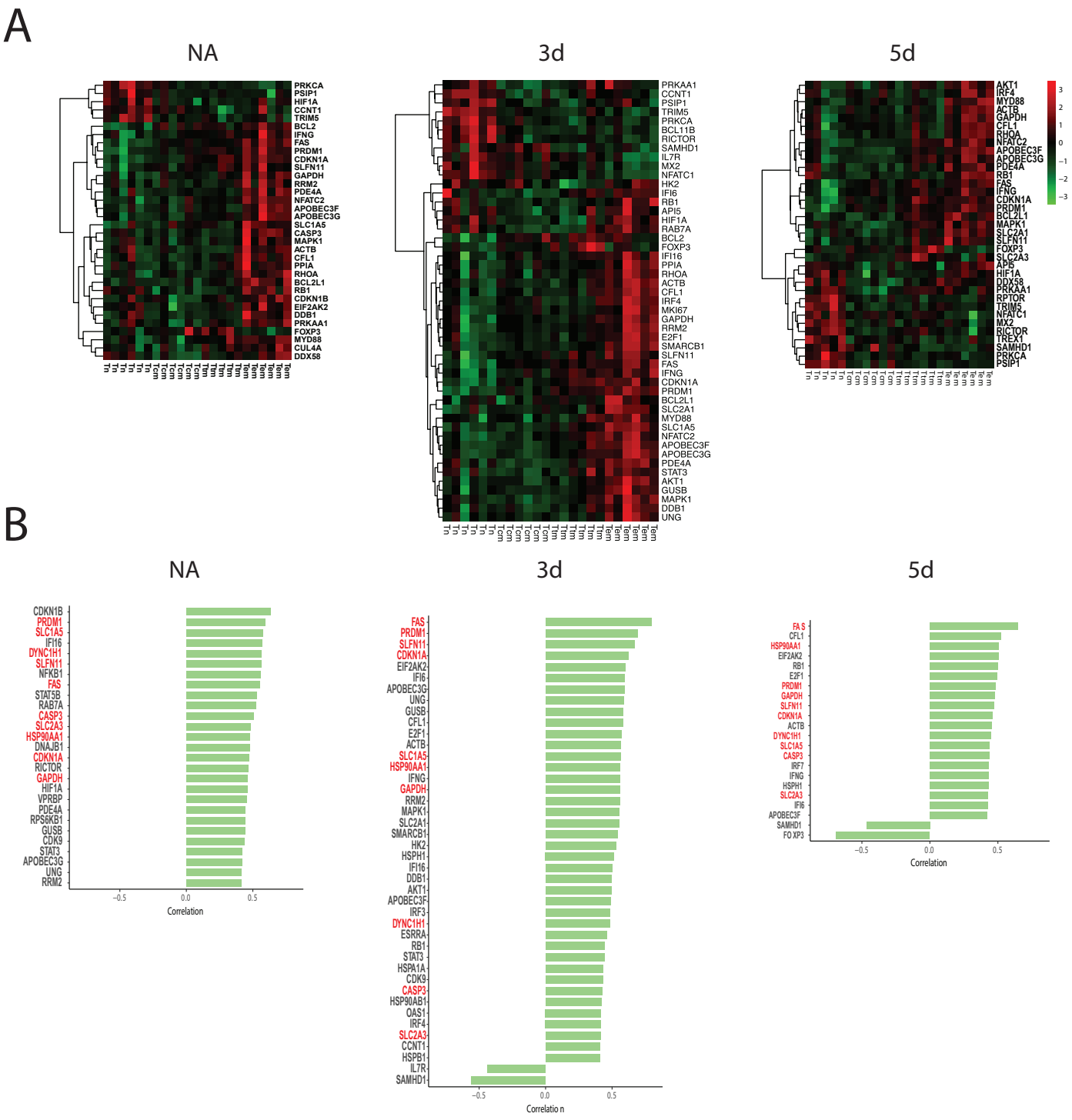

Figure 2

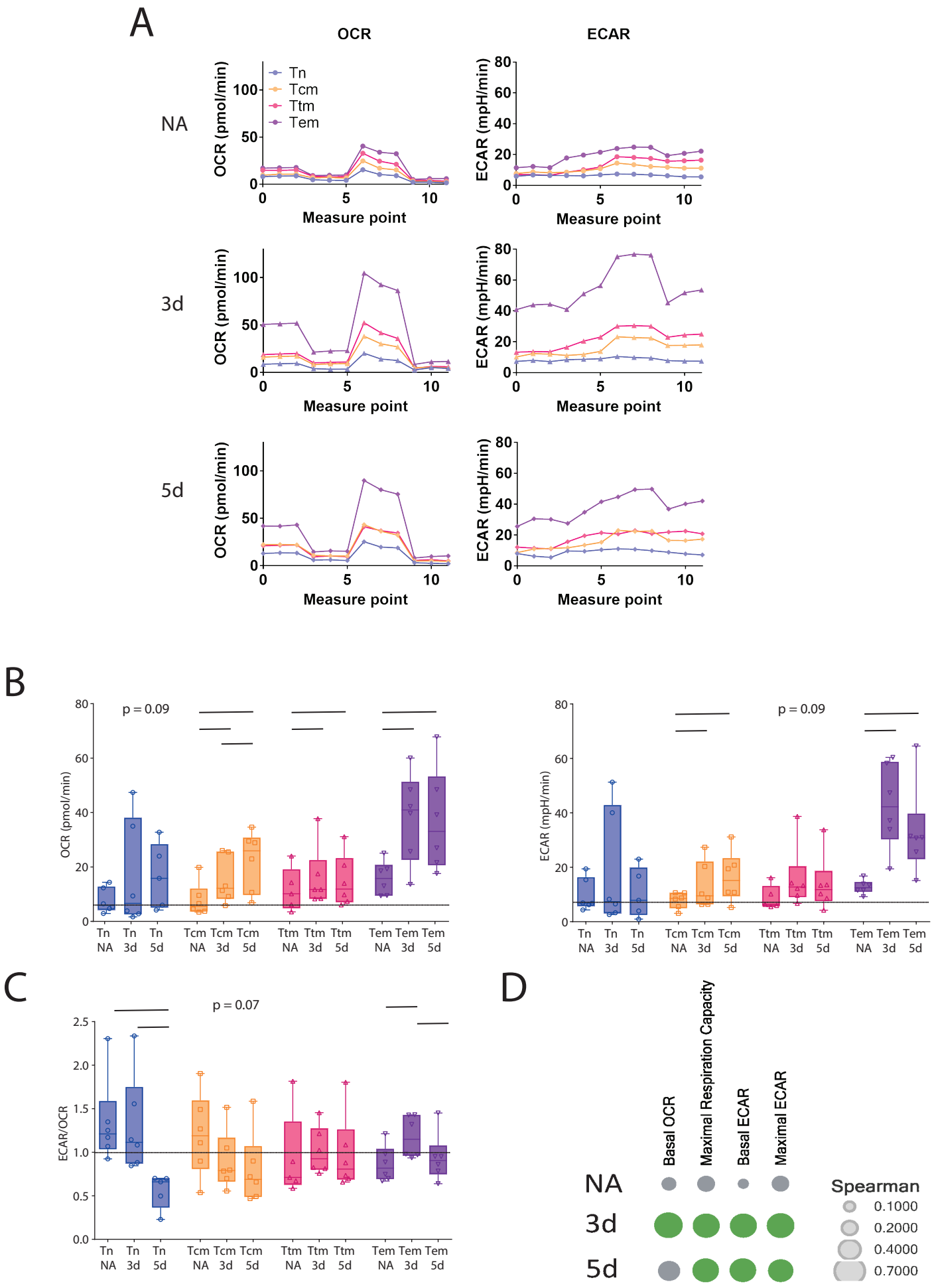
A
OCR
ECAR
NA
3d
5d
Tn
Tcm
Ttm
Tem
OCR (pmol/min)
ECAR (mpH/min)
Measure point
B
p = 0.09
OCR (pmol/min)
ECAR (mpH/min)
Tn NA
Tn 3d
Tn 5d
Tcm NA
Tcm 3d
Tcm 5d
Ttm NA
Ttm 3d
Ttm 5d
Tem NA
Tem 3d
Tem 5d
C
p = 0.07
ECAR/OCR
D
Basal OCR
Maximal Respiration Capacity
Basal ECAR
Maximal ECAR
Spearman
0.1000
0.2000
0.4000
0.7000

Figure 3

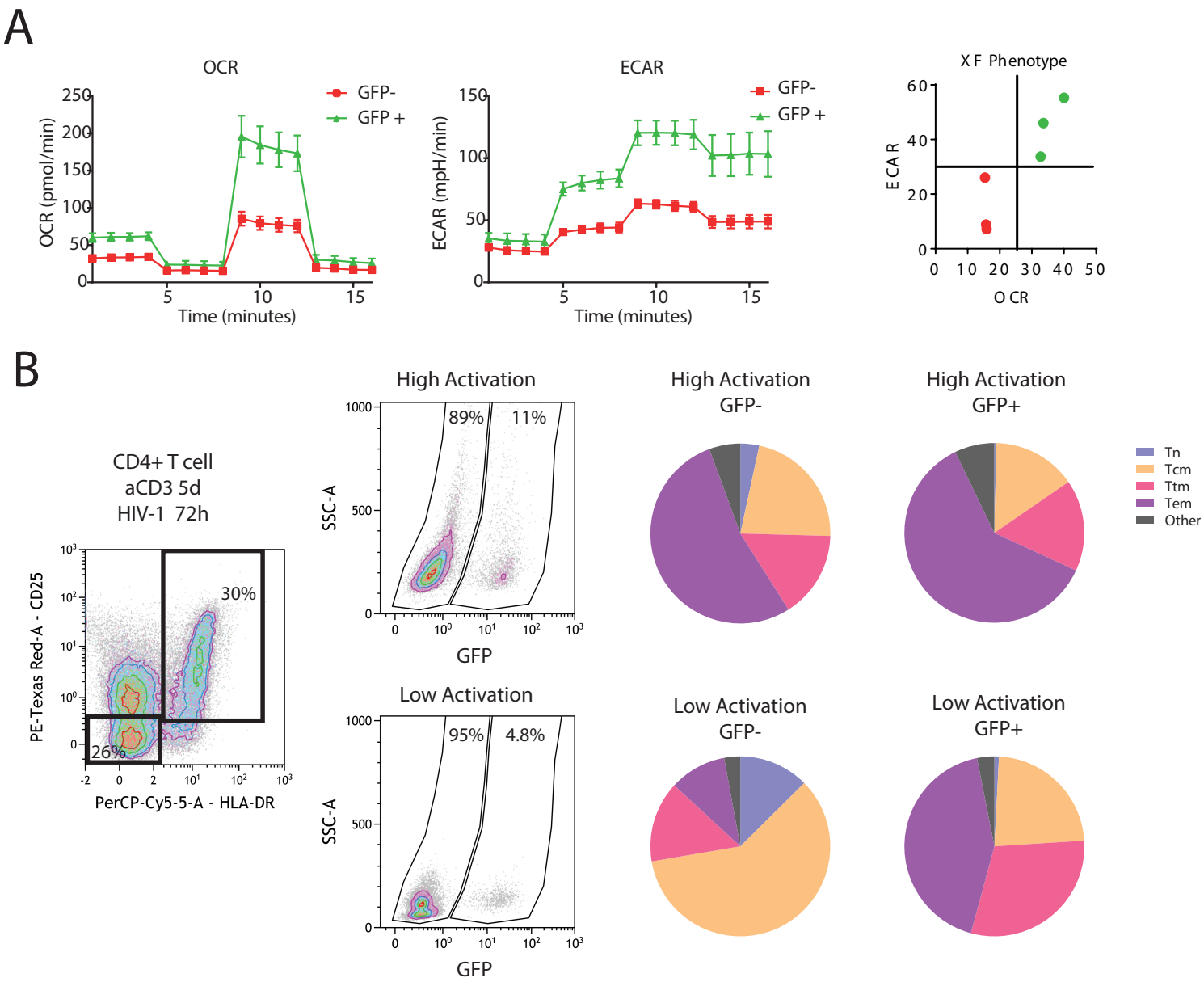
A
OCR
GFP-
GFP +
OCR (pmol/min)
Time (minutes)
ECAR
ECAR (mpH/min)
XF Phenotype
ECAR
OCR
B
CD4+ T cell
aCD3 5d
HIV-1 72h
PE-Texas Red-A - CD25
PerCP-Cy5-5-A - HLA-DR
30%
26%
High Activation
89%
11%
SSC-A
GFP
Low Activation
95%
4.8%
High Activation GFP-
High Activation GFP+
Low Activation GFP-
Low Activation GFP+
Tn
Tcm
Ttm
Tem
Other
C
High Activation
GFP+
GFP-
OCR (pmol/min)
Measure point
ECAR (mpH/min)
OCR (pmoles/min)
p = 0.027
OCR Basal
p = 0.051
Basal ECAR
Low Activation
GFP+
GFP -
p = 0.011
p = 0.050

Figure 4

A

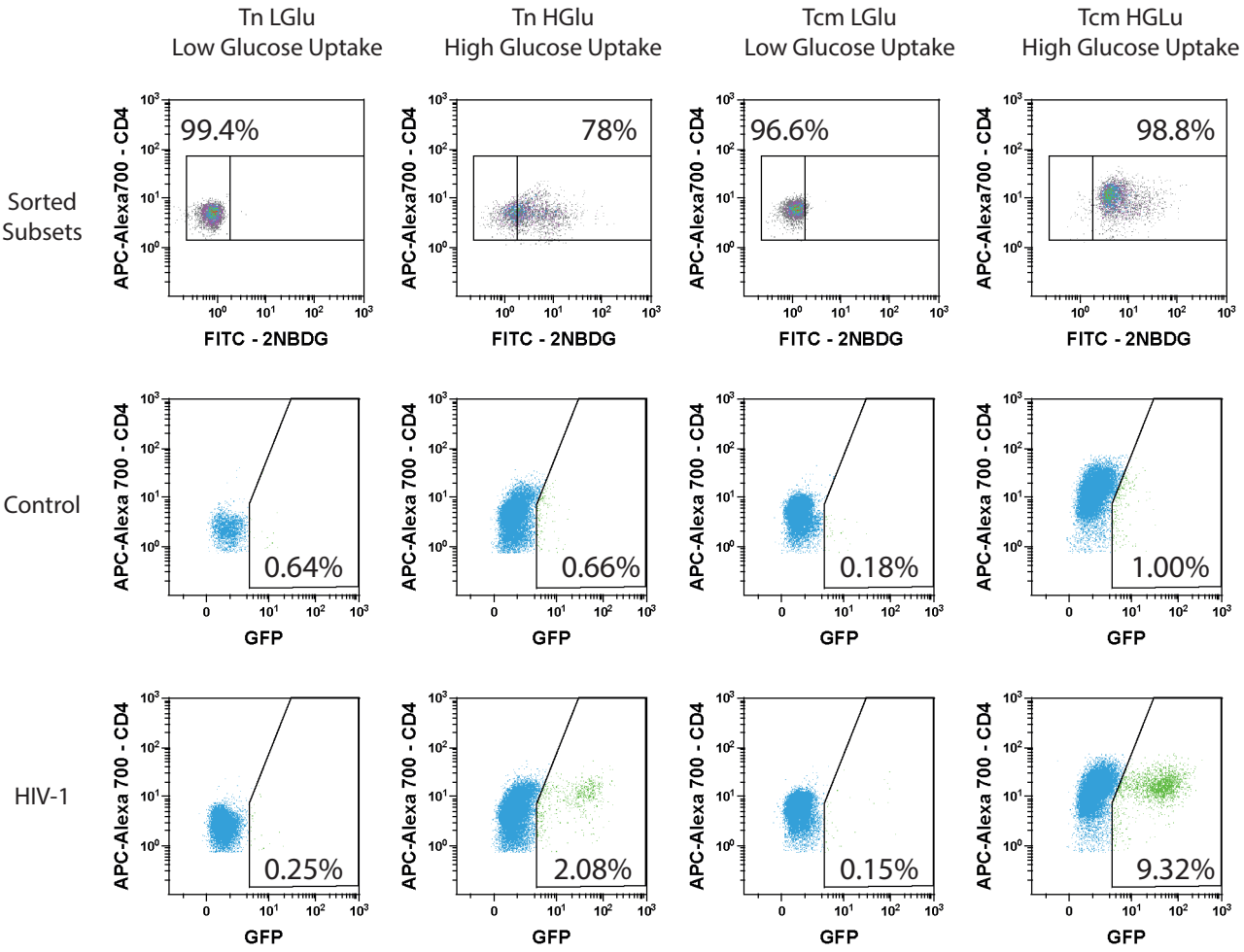
Tn LGlu
Low Glucose Uptake
Tn HGlu
High Glucose Uptake
Tcm LGlu
Low Glucose Uptake
Tcm HGLu
High Glucose Uptake
Sorted Subsets
Control
HIV-1
APC-Alexa700 - CD4
APC-Alexa 700 - CD4
FITC - 2NBDG
GFP
99.4%
78%
96.6%
98.8%
0.64%
0.66%
0.18%
1.00%
0.25%
2.08%
0.15%
9.32%

B

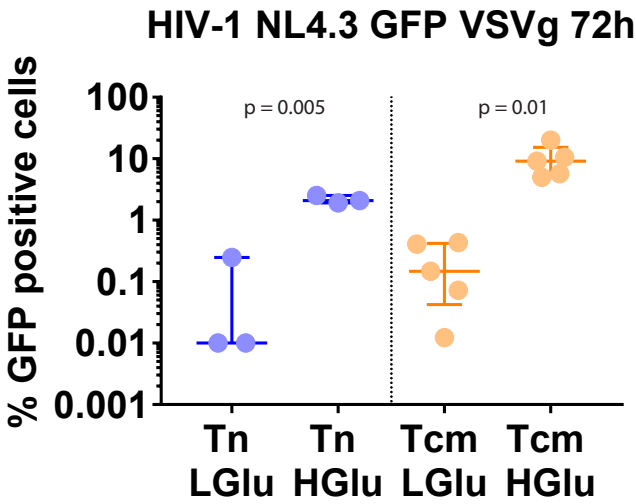
HIV-1 NL4.3 GFP VSVg 72h
% GFP positive cells
100
10
1
0.1
0.01
0.001
p = 0.005
p = 0.01
Tn LGlu
Tn HGlu
Tcm LGlu
Tcm HGlu

Figure 5

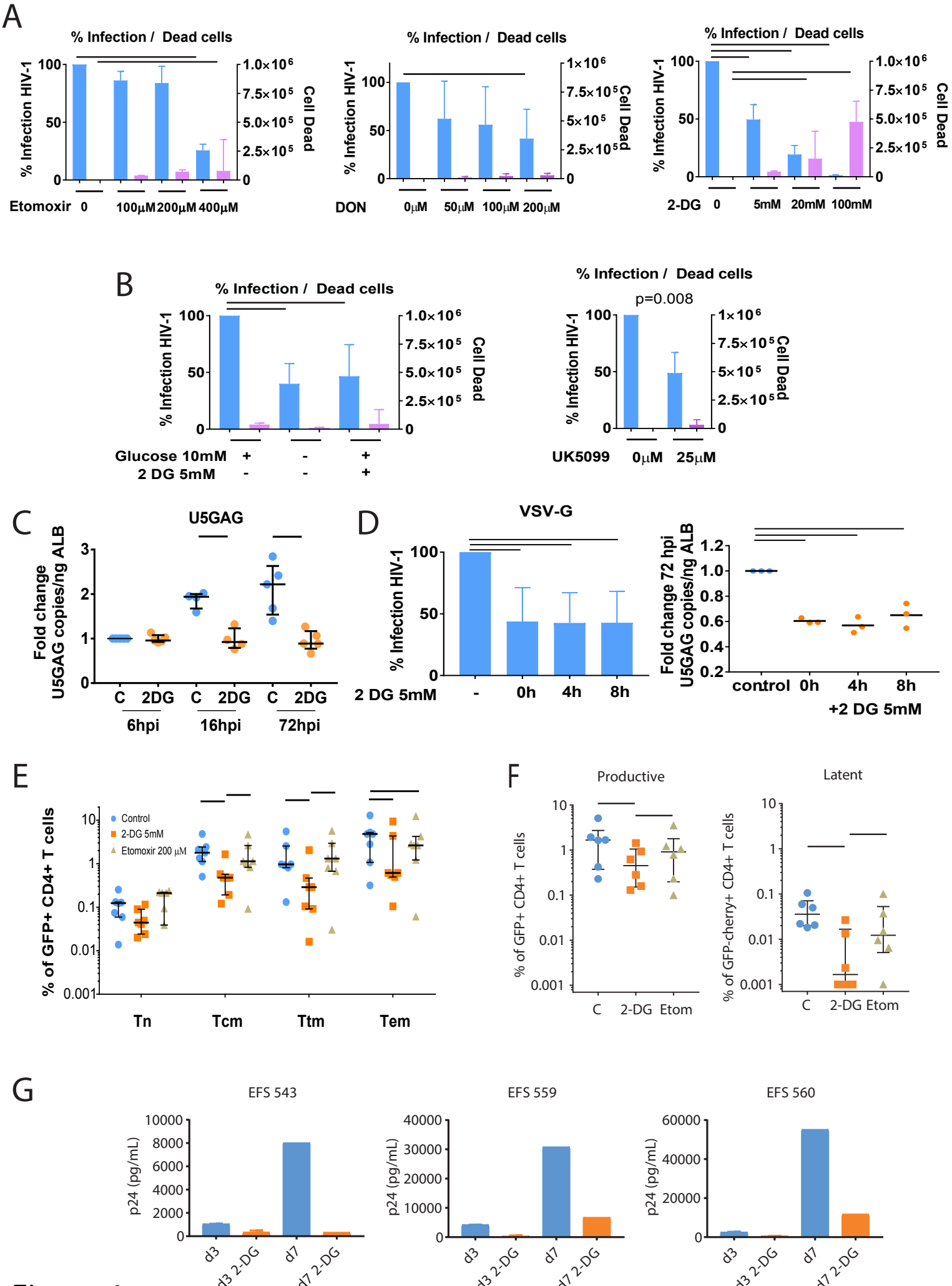
A
% Infection / Dead cells
% Infection HIV-1
Cell Dead
Etomoxir 0 100µM 200µM 400µM
DON 0µM 50µM 100µM 200µM
2-DG 0 5mM 20mM 100mM
B
Glucose 10mM + - +
2 DG 5mM - - +
p=0.008
UK5099 0µM 25µM
C
U5GAG
Fold change U5GAG copies/ng ALB
C 2DG C 2DG C 2DG
6hpi 16hpi 72hpi
D
VSV-G
2 DG 5mM - 0h 4h 8h
Fold change 72 hpi U5GAG copies/ng ALB
control 0h 4h 8h
+2 DG 5mM
E
% of GFP+ CD4+ T cells
Control
2-DG 5mM
Etomoxir 200 µM
Tn Tcm Ttm Tem
F
Productive
Latent
% of GFP-cherry+ CD4+ T cells
C 2-DG Etom
G
EFS 543
EFS 559
EFS 560
p24 (pg/mL)
d3 d3 2-DG d7 d7 2-DG

Figure 6

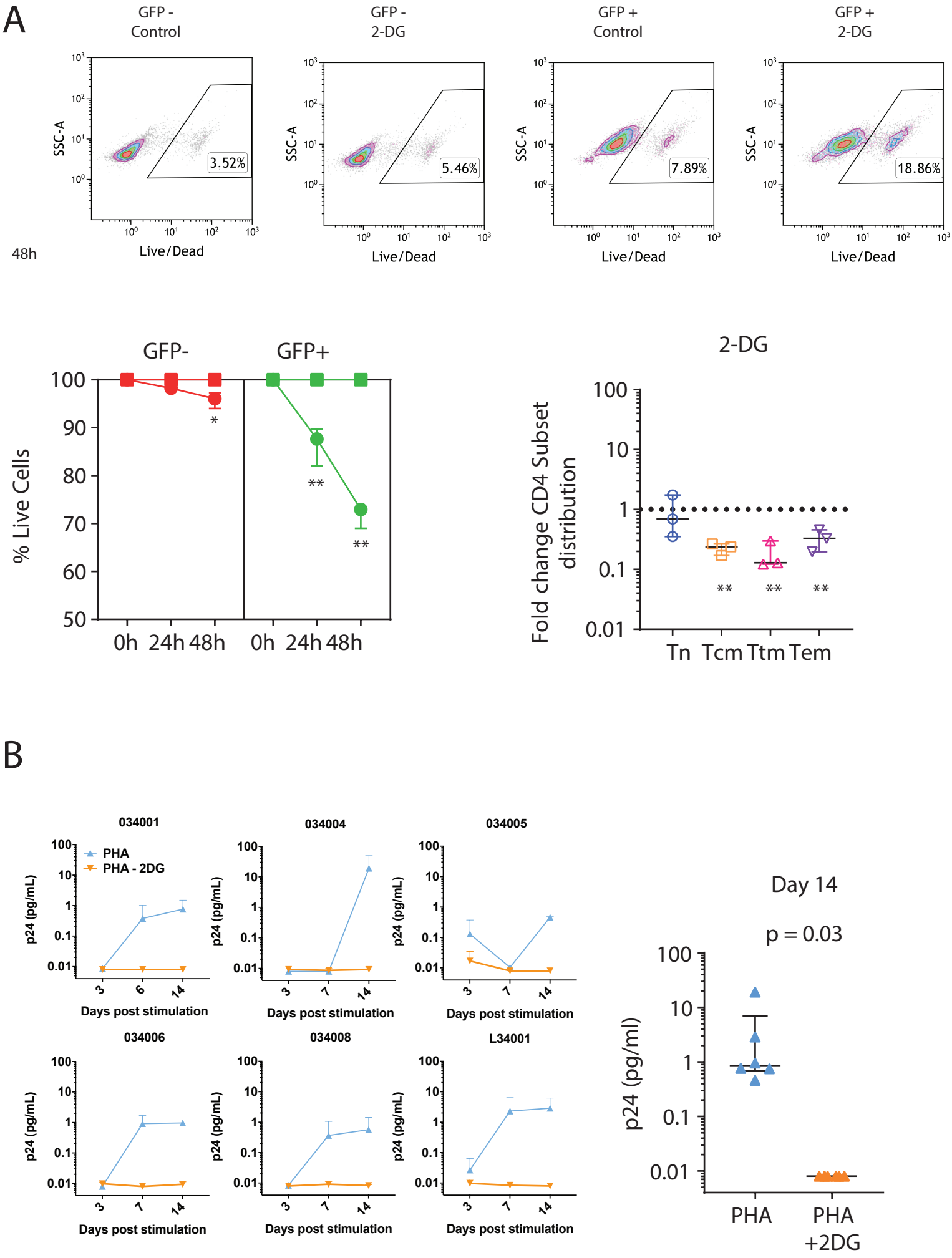
A
GFP -
Control
GFP -
2-DG
GFP +
Control
GFP +
2-DG
SSC-A
Live/Dead
3.52%
5.46%
7.89%
18.86%
48h
GFP-
GFP+
% Live Cells
0h 24h 48h 0h 24h 48h
2-DG
Fold change CD4 Subset distribution
Tn Tcm Ttm Tem
B
034001
034004
034005
034006
034008
L34001
PHA
PHA - 2DG
p24 (pg/mL)
Days post stimulation
Day 14
p = 0.03
p24 (pg/ml)
PHA
PHA +2DG

Figure 7

Oxphos
glycolysis

HIV-1
susceptible

HIV-1
resistant

Naive

Central
memory

Transitional
memory

Effector
memory

CD4+ T cells

Glutamine

DON

TCA

UK5099

Pyruvate

2DG

Lactate

GLUT

Glucose

Blocks
early steps of
HIV-1 replication

Eliminates recently
infected cells

Impairs viral spread